Università degli Studi di Pisa

DIPARTIMENTO DI FISICA 'E. FERMI'
Corso di Laurea Magistrale in Fisica

Tesi di Laurea Magistrale

Many-Body physics of strongly interacting Rydberg atoms

Candidato:
Guido Masella

Relatore:
Prof. Oliver Morsch

Anno Accademico 2014-2015

Contents

List of Figures

Introduction

The study of large assemblies of interacting particles is one of the most challenging tasks in physics. Even when the laws that govern the behaviour of the constituents of these system are simple, the understanding of the *emergent phenomena* in such large systems can be extremely complex. Many-Body physics is the field of study which tries to synthesize the governing principles of the macroscopic behaivour of such systems from the microscopic laws [1]. The basic concepts of the Many-Body physics are summarized in "The more is different" [2] by the Nobel laureate (in 1977) Philip Warren Anderson:

> "The behavior of large and complex aggregations of elementary particles, it turns out, is not to be understood in terms of a simple extrapolation of the properties of a few particles. Instead, at each level of complexity entirely new properties appear, and the understanding of the new behaviors requires research which I think is as fundamental in its nature as any other."

The understanding of the dynamics out of equilibrium of stongly interacting many-body systems is nowadays an active field of study but many problems remain unsolved because of the limit of the analytical and numerical tools used. The development in this field is carried out by the availability of highly controllable experimental platforms to probe such problems. [3]. Rydberg atoms, which are atoms excited to states with high principal quantum number, have proved to be a very successful platform for the study of these systems because of the precise control of parameters and interactions of the system [4].

In the present thesis the emergent properties of a many-body system are studied in condi-

tions where the dynamics of the internal and external degrees of freedom of the constituent particles can be partially decoupled. The study is done by means of Monte Carlo simulations upon a simple toy model.

Internally the system is modelled as an Ising-like spin system [5] coupled to an external field and with long range interactions among the spins. Dissipation is also included in the model, and a master equation approach is used to derive the time evolution of the system. Different Kinetic Monte Carlo methods are discussed in order to solve that master equation.

We used the model and the methods developed to study emergent phenomena in the excitation dynamics of a cold gas of Rydberg atoms [6]. In the resonant regime we observed the effects of the so-called dipole blockade [7] where the presence of an excited atom inhibits the excitation of its neighbors. In the off resonant regime we observed facilitated excitation, whereby an excitation in the system shifts a ground state atom at a well-defined distance into resonance. We also performed simulations of the excitation process with quenches of the detuning, finding unexpected results in the dynamics approaching equilibrium.

The dynamics of the external (translational) degrees of freedom is modelled as that of classical particles which interact by means of a potential of the form C_α/r^α. The features of different algorithms to solve the classical equations of motion are discussed focusing on the requirement that the Hamiltonian must be conserved while integrating the Hamilton equations for such systems.

In order to test the algorithm we performed simulations on the external dynamics of a cluster of Rydberg atoms replicating the features of an experiment performed in the laboratory at Pisa. That experiment aims to observe directly the effect of van der Waals forces between atoms of Rubidium excited to Rydberg states. We used the simulations to analyze the outcome of the experiment and found good agreement between the experimental data and the simulation.

My contribution to the work presented in this thesis consisted in the development and in the implementation of the simulation methods and models discussed. The *core* set of libraries

and software developed can be used to simulate the dynamics out of equilibrium for different kind of systems which spans from regular lattices of Ising-spin system in one, two or three dimensions to the strongly interacting gasses of Rydberg atoms which can be obtained in laboratory using modern trapping techniques.

Furthermore I contributed to the following publication: R. Faoro, C. Simonelli, M. Archimi, G. Masella, M. M. Valado, E. Arimondo, R. Mannella, D. Ciampini, O. Morsch, *"Van der Waals explosion of cold Rydberg clusters"*, arXiv:1506.08463, (2015), which is under review at Physical Review Letters.

Chapter 1

Theoretical Foundations

The work presented in this thesis has been done aiming to study the behavior of a very specific physical system that is a cold gas of Rydberg atoms. The toy model used to approach this study, however, as well as the methods and the algorithm used, is largely independent of the actual physical system. This toy model is a system of many (N) interacting particles in an external field.

This chapter is dedicated to the development of the model and of the equations which govern its time evolution. The discussion is split in two different parts, one about the dynamics of the internal degrees of freedom of the particles and one about the dynamics of the external (i.e., translational) ones.

1.1 Internal degrees of freedom

We assume that the particles which compose our system can be modelled as two level systems, just like (pseudo) spin1/2 particles. The two allowed states will be then referred to as $|\uparrow\rangle$ and $|\downarrow\rangle$.

Also for this system we assume the Hamiltonian

$$H = h_x \sum_k^N \sigma_x^k + h_z \sum_k^N n_k + \sum_{km}^N V_{km}^\alpha \tag{1.1}$$

where $\{\sigma_x^k, \sigma_y^k, \sigma_z^k\}$ are the Pauli matrices, $n_k = (1 - \sigma_z^k)/2$ is the number operator of the kth particle and the interaction among the spins is given by

$$V_{km}^\alpha = C_\alpha \frac{n^k n^m}{d(k,m)^\alpha} \tag{1.2}$$

with and $d(k,m)$ the distance between two particles. This hamiltonian describes an Ising-like spin model in an external mixed transverse and longitudinal field $(h_x,\ h_z)$ [8] (also see [9] as an example of such system).

The derivation presented in this chapter of the laws which govern the time evolution for such a system, follows from the discussion presented by *Lesanovsky et al.* [10].

If ρ is the reduced density matrix of a single particle its time evolution is given by the *Von Neumann* equation [11, p. 110]

$$\frac{\partial \rho}{\partial t} = -\imath[H, \rho] \tag{1.3}$$

While the equation (1.3) gives the correct evolution for a closed system it does not hold in the presence of dissipation. In this case the time evolution of the system is given by a more general master equation

$$\frac{\partial \rho}{\partial t} = -\imath[H, \rho] + \tilde{\gamma} \sum_k \left(n_k \rho n_k - \frac{1}{2}\{n_k, \rho\} \right) \tag{1.4}$$

which is said to be in *Lindblad* form [12, 13]. Here $\tilde{\gamma}$ is the rate at which the *dephasing* of the state $|\uparrow\rangle$ with respect to the state $|\downarrow\rangle$ occurs. The Lindblad master equation (1.4) is clearly local in time. Moreover, it is also Markovian.

The hamiltonian (1.1) can be split in two parts $H = H_x + H_z$ where $H_x = h_x \sum \sigma_x^k$ is the interaction of the system with the transversal component of the field. This allows us to write also the master equation in split form

$$\frac{\partial \rho}{\partial t} = \mathcal{L}_x \rho + \mathcal{L}_z \rho \tag{1.5}$$

where

$$\mathcal{L}_x\rho = -\imath[H_x, \rho] \tag{1.6}$$

$$\mathcal{L}_z\rho = -\imath[H_z, \rho] + \tilde{\gamma}\sum\left(n_k\rho n_k - \frac{1}{2}\{n_k, \rho\}\right) \tag{1.7}$$

We are interested in the study of this system when $\mathcal{L}_z$ is dominant over $\mathcal{L}_x$ which corresponds to the case when the dephasing rate is large: $\tilde{\gamma} >> |h_x|$ and the dynamics governed by $\mathcal{L}_x$ is thus faster than the dynamics under $\mathcal{L}_z$. [10] The aim of this study is to resolve the slow dynamics of the system.

In this case the operator $\mathcal{P} = \lim_{t\to\infty} e^{\mathcal{L}_z t}$ is a projector on the subspace where the slow dynamics takes place. It is also true that $\mu \equiv \mathcal{P}\rho$ is diagonal, so that the coherences (i.e., off-diagonal terms of the density matrix) are removed from the density-matrix μ, which becomes a classical state.

Under these considerations the master equation (1.4) can be simplified and reduced to an effective classical one

$$\frac{\partial\mu}{\partial t} = \sum_k^N \Gamma_k(\sigma_x^k\mu\sigma_x^k - \mu) \tag{1.8}$$

where the transition rates are given by

$$\Gamma_k = 4\frac{h_x^2}{\tilde{\gamma}}\frac{1}{1 + \frac{4}{\tilde{\gamma}^2}[h_z - V_\alpha(k)]^2} \tag{1.9}$$

where $V_\alpha(k) = \sum_{m\neq k}\frac{C_\alpha n_m}{d(m,k)^\alpha}$ is the potential upon the spin k.

From the equation (1.9) we can recognize two different regimes: one for an only transversal external field ($h_z = 0$) and the other when the field has also a nonzero longitudinal component of the field ($h_z \neq 0$).

1.1.1 Rydberg atoms

The discussion in the present thesis is focused to the study of system of Rydberg atoms which are atoms excited to states with high principal quantum number n, and, therefore, a

large polarizability which leads to strong interactions between such atoms. These atoms can be modelled as a two level system where the $|\downarrow\rangle$ is their (non-interacting) ground state and $|\uparrow\rangle$ is the (interacting) excited Rydberg state. Assuming that the atoms only interact with an external laser field and with each other trough a two-atom potential, the Hamiltonian of the system can be expressed, in the *rotating frame approximation* as

$$H = -\Delta \sum_k n_k + \frac{\Omega}{2} \sum_k \sigma_x^k + \sum_{m \neq k} \frac{C_\alpha n_k n_m}{d(k,m)^\alpha} \tag{1.10}$$

with Ω the Rabi frequency and Δ the detuning of the laser. [14, 15]

For these atoms the rates of equation (1.9) become

$$\Gamma_k = \frac{\Omega^2}{\gamma} \frac{1}{1 + \left(\frac{\Delta - V_k}{\gamma}\right)^2} \tag{1.11}$$

where γ indicates the linewidth of the laser.

So for Rydberg atoms the Rabi frequency Ω corresponds to the strength of the transversal field h_x while the detuning Δ corresponds to the strength of the longitudinal field h_z as can be seen comparing the two hamiltonians (1.1) and (1.10).

1.1.2 Blockade

When only the transversal component of the field is present (ie. $h_z = 0$) the rates becomes

$$\Gamma = 4 \frac{h_x^2 \gamma}{\gamma^2 + 4V_\alpha(k)^2} \tag{1.12}$$

Consider a system composed by only two spins at a given distance r. The potential $V_\alpha(2)$ on the second spin will be always zero if the first one is in the state $|\downarrow\rangle$ while it will be different in the opposite case. This means that the rate Γ_2 of the second spin will be equal to $4\frac{h_x^2}{\gamma}$ when the first spin is in the state $|\downarrow\rangle$. In the opposite case the rates will depend on the potential and will be lower for higher V_α and higher for low V_α. The form of the rates as a function of the distance between two particles is shown in Figure 1.1.

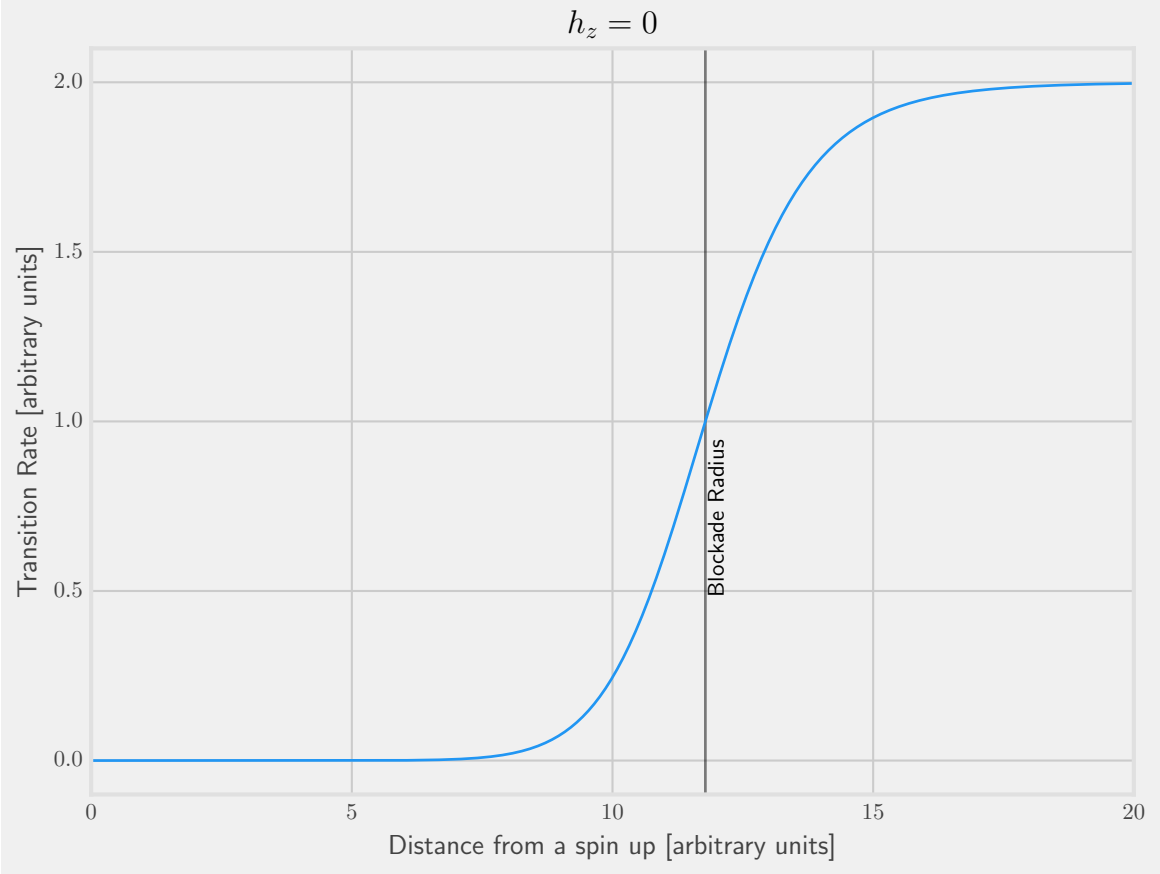

FIGURE 1.1. *Transition rates in the case where $h_z = 0$. The rate Γ_k is plotted as a function of the distance r from a spin in the state $|\uparrow\rangle$. The potential is taken to be $\propto 1/r^6$.*

In terms of the distances, the transitions near a spin already in the state $|\uparrow\rangle$ will be highly suppressed. This effect is called *blockade* [7] because the existing spin in the state $|\uparrow\rangle$ effectively blocks the excitation of its neighbours. A characteristic length called *blockade radius* can be defined to be the distance from a spin in the "up" state where the rate is at half of its maximum value. This blockade radius is thus found to be

$$R_b = \left(\frac{2C_\alpha}{\tilde{\gamma}}\right)^{\frac{1}{\alpha}} \tag{1.13}$$

Consider a chain of spins where the distances are lower than the blockade radius. If a "spin up", namely a spin in state $|\uparrow\rangle$, is already present in the chain, the transitions of all its neighbors (up to the distance R_b) will be inhibited. This effect results in a slowing down of the dynamics with respect to a system of noninteracting spins or with respect to the case where the distance of the spins in the chain are greater than R_b.

In the case of Rydberg atoms an example of this effect is given in Figure 1.2. In the presence of an excitations all the $|\uparrow\rangle$ of nearby atoms are shifted by the effects of the potential suppressing the excitation of nearby atoms.

1.1.3 Facilitation

An effect opposite to the blockade can be seen when the external field has a longitudinal component, in other words when $h_z \neq 0$ in equation (1.1).

The first thing to be observed is the fact that the rates have their maximum value not when the potential V_α is zero but when it is equal to h_z. As can be seen from Figure 1.3 the spins at a for which $V_\alpha = h_z$ have higher rates and so their transitions are more probable, *facilitated*.

For a system of only two spins, the distance at which the *facilitation* condition is satisfied is called *facilitation radius* and it is given by

$$r_{\text{fac}} = \left(\frac{C_\alpha}{h_z}\right)^{\frac{1}{\alpha}} \tag{1.14}$$

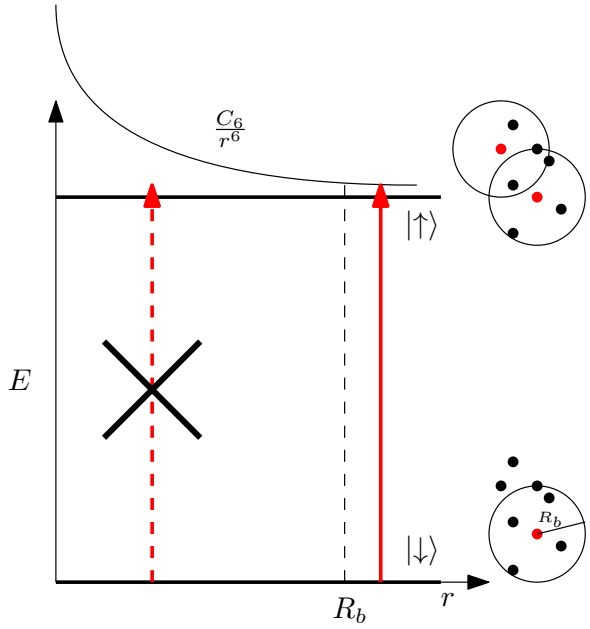

FIGURE 1.2. *Representation of the blockade for Rydberg atoms. The presence of an excitation suppress the formation of other excitations for distances less than the blockade radius R_b.*

It is useful to observe that stronger fields (in the longitudinal component) correspond to a shorter facilitation radius.

To investigate further the *facilitation* effect consider a chain of spins in a given external field and with the step of the chain being equal to the facilitation radius. If all the spins are in the state $|\downarrow\rangle$ the dynamics when $h_z \neq 0$ is slower with respect to the case when $h_z = 0$ and all the transitions are less probable at distance r_{fac}. On the contrary, when a "spin up" is present, the transitions of its first neighbors will be more probable. At one point the neighbors will do the transition towards the state $|\uparrow\rangle$ and then their neighbors will be facilitated. So the presence of a single "spin up" will start a chain reaction trough the entire chain with a consequent speedup of the dynamics.

As can be seen from Figure 1.3, for a given external field h_z the rates are different from zero not only in correspondence of the facilitation radius but also in a small range around

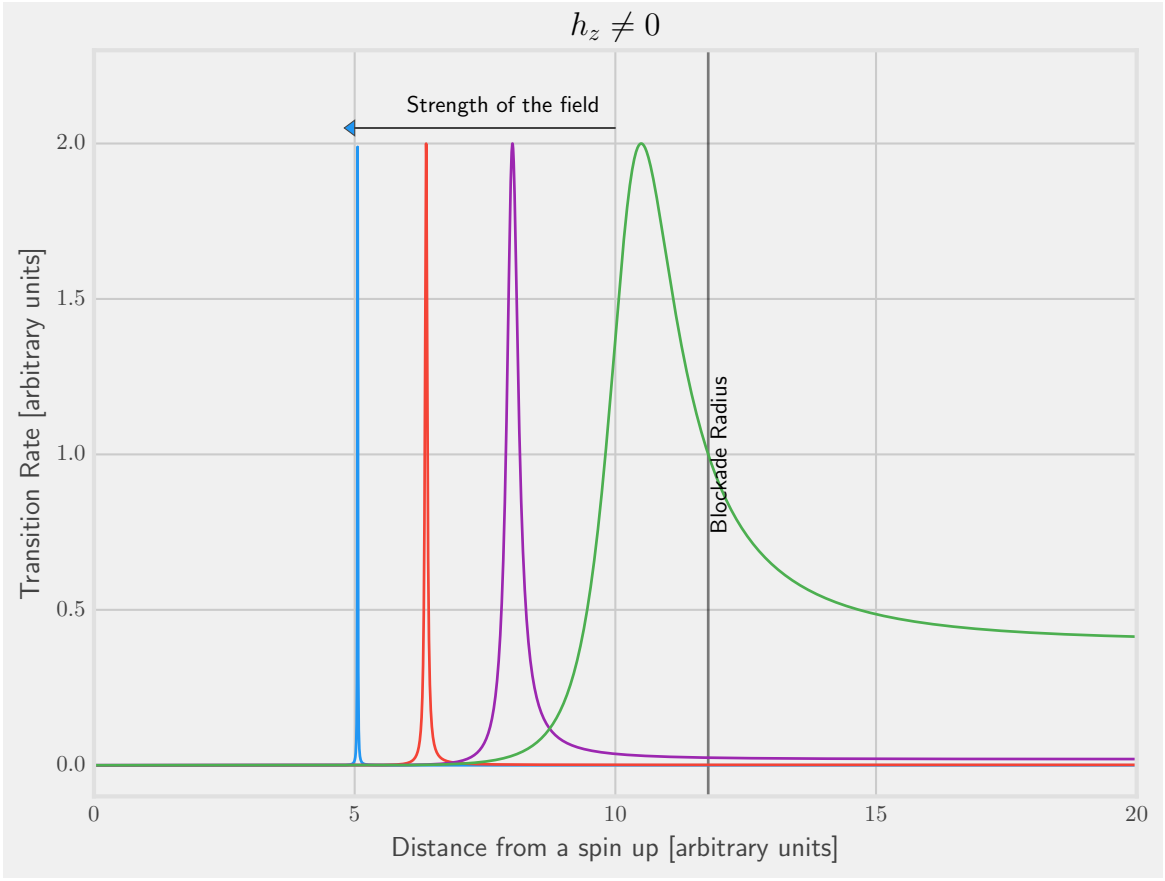

FIGURE 1.3. *The transition rate Γ_k for a given spin is plotted as a function of the distance r from another spin in the state $|\uparrow\rangle$ when the external field has a longitudinal component. The potential is taken to be $\propto 1/r^6$. The blockade radius is indicated for the only purpose of comparison*

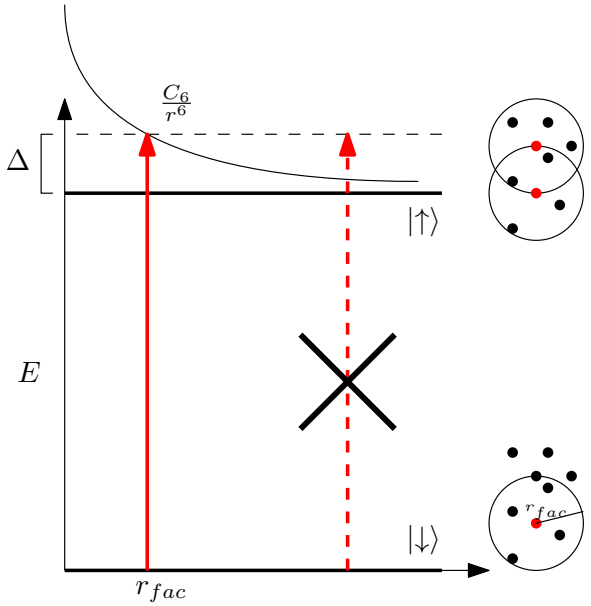

FIGURE 1.4. *Schematic of the facilitation effect for a system of Rydberg atoms excited off-resonance with the detuning Δ. The presence of an atom in the Rydberg state facilitates the dynamics of the atoms at a distance equal to the facilitation radius.*

it. The length of this range, which corresponds to the width of each peak in Figure 1.3 is given by

$$\Delta r_{\text{fac}} = r_{\text{fac}} \times \frac{\tilde{\gamma}}{2\,\alpha\,h_z} \tag{1.15}$$

1.1.4 Stationary state

Even if the greatest interest in the present thesis is on the dynamics *approaching* the equilibrium, information on the stationary state will be useful in the analysis of the numerical simulations. The stationary state μ_s ($\partial_t \mu_s = 0$) can be easily found from equation (1.8) to be the one that satisfies

$$\sigma_x^k \mu_s \sigma_x^k = \mu_s \tag{1.16}$$

which is true only if μ_s is the completely mixed state. So the stationary state is expected to be the one for witch the probability $p_{|\uparrow\rangle}$ to find a given spin in state $|\uparrow\rangle$ is equal to the

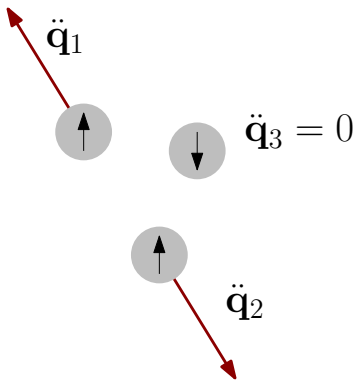

FIGURE 1.5. *Using the potential written in (1.17) the interaction is present only if two atoms are both in the state* $|\uparrow\rangle$.

probability $p_{|\downarrow\rangle}$. In terms of Rydberg atoms, this will correspond to a state in which half of the atoms in the system are (on average) excited.

1.2 External degrees of freedom

Externally each particle is modelled as a point mass with defined classical position and momentum. Only particle in the "spin up" state will interact while the interactions between $|\uparrow\rangle$, $|\downarrow\rangle$ and between two particles in the "spin down" state are absent (see Figure 1.5). The Hamiltonian which governs the external dynamics is given by

$$\mathcal{H} = T(\boldsymbol{p}_1, \ldots, \boldsymbol{p}_N) + V(\boldsymbol{q}_1, \ldots, \boldsymbol{q}_N) = \sum_k^N \frac{\boldsymbol{p}_k^2}{2m_k} + \sum_k^N \sum_{m \neq k}^N \frac{C_\alpha n_k n_m}{|\boldsymbol{q}_k - \boldsymbol{q}_m|^\alpha} \tag{1.17}$$

where $\{\boldsymbol{q}_k\}$ and $\{\boldsymbol{p}_k\}$ are the position and momentum vectors of the particles and n_k is equal to 1 if the internal state of the kth particle is $|\uparrow\rangle$ and 0 otherwise.

The time evolution of this system is given by the Hamilton equations

$$\frac{d\boldsymbol{p}_k}{dt} = -\frac{\partial \mathcal{H}}{\partial \boldsymbol{q}_k} \tag{1.18}$$

$$\frac{d\boldsymbol{q}_k}{dt} = \frac{\partial \mathcal{H}}{\partial \boldsymbol{p}_k} \tag{1.19}$$

which, given the form of the Hamiltonian (1.17), can be reduced to the equations

$$\ddot{\boldsymbol{q}}_k = -\frac{\boldsymbol{\nabla}_k V}{m} \tag{1.20}$$

1.3 Coupled dynamics

When the dynamics of the internal degrees of freedom is frozen (the particles cannot change their internal state), each particle behaves classically with the dynamics governed by the Newton's equations of motion (1.20). On the contrary, if the external dynamics is frozen and the positions of the particles are fixed the internal dynamics is governed only by the equations (1.8).

What happens in the case of a cloud of particles, free in real space in the presence of a nonzero external field, is that the dynamics of internal and external degrees of freedom is coupled. As can be seen from equation (1.9) the dependence of the particles positions on time implies the dependence of the rates on time. On the other hand, the dependence on time of the "occupation numbers" n_k in equation (1.17) implies a time dependence of the potential and hence in the Hamiltonian.

A way to solve this coupled dynamics is using Monte Carlo integration to simulate many times the evolution of the system and then averaging all these samples to obtain the solutions of the equation (1.8). This approach is based on the assumption that a (statistically) valid evolution of the internal degrees of freedom is given by a sequence of transitions, namely spin flips, at times sampled from an appropriate distribution

$$(t_1, k_1) \longrightarrow (t_2, k_2) \longrightarrow \ldots \longrightarrow (t_i, k_i) \longrightarrow \ldots \tag{1.21}$$

Between different transitions the internal state of the system will remain the same and so the external dynamics (i.e., between t_i and t_{i+1}) can be easily integrated from equations (1.20).

Chapter 2

Algorithms for many-body computations

Numerical simulations are a fundamental tool in the understanding of many-body systems but at the same time they are challenging both in terms of performance and numerical precision.

The discussion in this Chapter is focused on the algorithms used to solve the equations of motion of both the internal and external dynamics of a many-body system. The class of Kinetic Monte Carlo algorithms is introduced as a reliable method to simulate the dynamics of the internal degrees of freedom of the system when their time evolution is described by a *master equation* for continuous-time Markov processes. Methods to resolve the classical hamiltonian dynamics of the external degrees of freedom are then discussed with particular interest on algorithms that ensure the conservation of energy for the system. Finally a discussion is made on how these two algorithms can work togheter to simulate the complete and detailed time evolution of the system.

2.1 Kinetic Monte Carlo methods

The Kinetic Monte Carlo (KMC) is a variant of Monte Carlo method designed to model the temporal evolution of a system through the examination of kinetic or procedural information about a stochastic sequence of fundamental processes.

The KMC method originates from the work of *Bortz, Kalos and Lebowitz* [16] where the authors introduced a new algorithm termed N-Fold Way (NFW) as a complementary method to the *Metropolis* algorithm [17] for simulations of Ising spin systems. While the latter is based on the idea to compute energies of a model system in randomly generated states weighting each state equally but biasing the state's selection with the likelihood of realizing it according to the Boltzmann energy equation, the NFW algorithm chooses and implements random transitions between the configurations of the system biasing the choice of the transition according to its likelihood.

Unlike the Metropolis method, the stochastic nature of the NFW is embodied in the incrementation of time. The main difference between the two algorithms is that in the NFW the duration of each step is a stochastic variable. The NFW method can reproduce not only the distribution of systems at equilibrium, like the Metropolis algorithm, but can also reproduce the time evolution of systems out of equilibrium.

The Kinetic Monte Carlo method is currently widely used in many fields of science, from the study of chemical reactions [18] and of the physics and chemistry of surfaces [19] to the simulation of processes of crystallization and crystal growth [20, 21]; from the study of vacancy-mediated diffusion in alloys [22] to the simulation of cold gases of Rydberg atoms [23, 10].

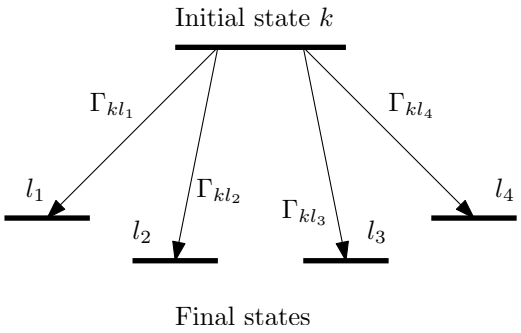

FIGURE 2.1. *Pictorial representiation of transition rates from a state k*

2.1.1 Formulation of the algorithm

Consider a classical system whose time evolution can be expressed in the form of a master equation

$$\frac{dP_k}{dt} = \sum_{l=1}^{N} \Gamma_{kl} P_l - \sum_{l=1}^{N} \Gamma_{lk} P_k \tag{2.1}$$

which represents the time evolution of the probability P_l of a system to be in the state l chosen from the set of the N possible states. Here Γ_{kl} represent the rate at which the transition process from one state k to the state l occurs, as can be seen in Figure 2.1

In the KMC method the transition from the current state k to the next one l is chosen so that

$$R_{l-1} < \rho_1 R_N \leq R_l \tag{2.2}$$

where the $R_j = \sum_{i=1}^{j} \Gamma_{kj}$ are the N partial sums of the rates and ρ_1 is a random number uniformly chosen in the interval $(0, 1]$. As can be seen in Figure 2.2 the length of each interval $(R_{j-1}, R_j]$ is equal to Γ_{kj} and this ensures that the probability of choosing the transition toward the j-th state is proportional to its rate so that more probable events will be picked more often than less probable ones.

After each step of the algorithm the time of the system is increased by the amount

$$\Delta t = -\frac{\ln \rho_2}{R_N} \tag{2.3}$$

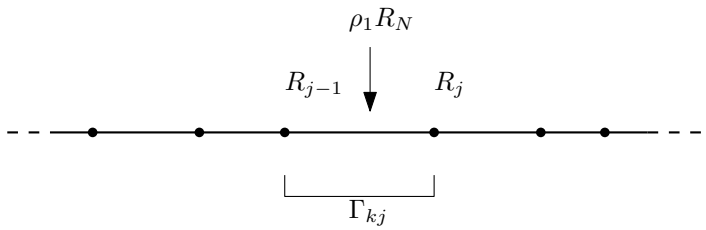

FIGURE 2.2. *Schematic representation of the choice of the transition. Each interval has length Γ_{kj} so the probability to choose a transition is proportional to its rate*

where ρ_2 is another randomly generated number in the interval $(0, 1]$. The duration of each time step is then proportional to the inverse of the sum of all the rates so that it will be shorter when the allowed transitions are more probable and longer in the opposite case.

When the transition toward the new state is performed and the configuration of the system is changed, the list of allowed transitions needs to be updated along with the rates and another step of the algorithm can be carried out. A schematic of the structure of the NFW algorithm can be seen in Figure 2.3

Time-dependent rates. The time of the system can be increased by the amount written in equation (2.3) when the rates depends only on the current configuration of the system and not explicitly on time. When an explicit dependence on time is present on scales comparable with the duration of each transition, the original NFW procedure is not useful anymore and needs to be generalized in the case when

$$\Gamma_{lk} \equiv \Gamma_{lk}(t). \tag{2.4}$$

Starting from a system in the state labeled k at time t, the direct integration of the equation (2.1) gives the probability $p_{\text{survival}}(t') = \exp\left[\int_t^{t'} R_N(\tau)\, d\tau\right]$ that the system has not yet escaped from the state k at time $t' = t + \Delta t$. So the probability that the system has escaped from the state k after a time Δt is $1 - p_{\text{survival}}(t')$ and is equal to the integral $\int_t^{t'} p(\tau)\, d\tau$ of the probability density $p(\tau)$ from which the new time of the system is sampled[1] The integrated

[1] The form of the probability density for the time step can be found by direct differentiation of $1 - p_{\text{survival}} = \int_t^{t'} p(\tau)\, d\tau$ and is $p(t') = R_N(t') \int_t^{t'} R_N(\tau)\, d\tau$

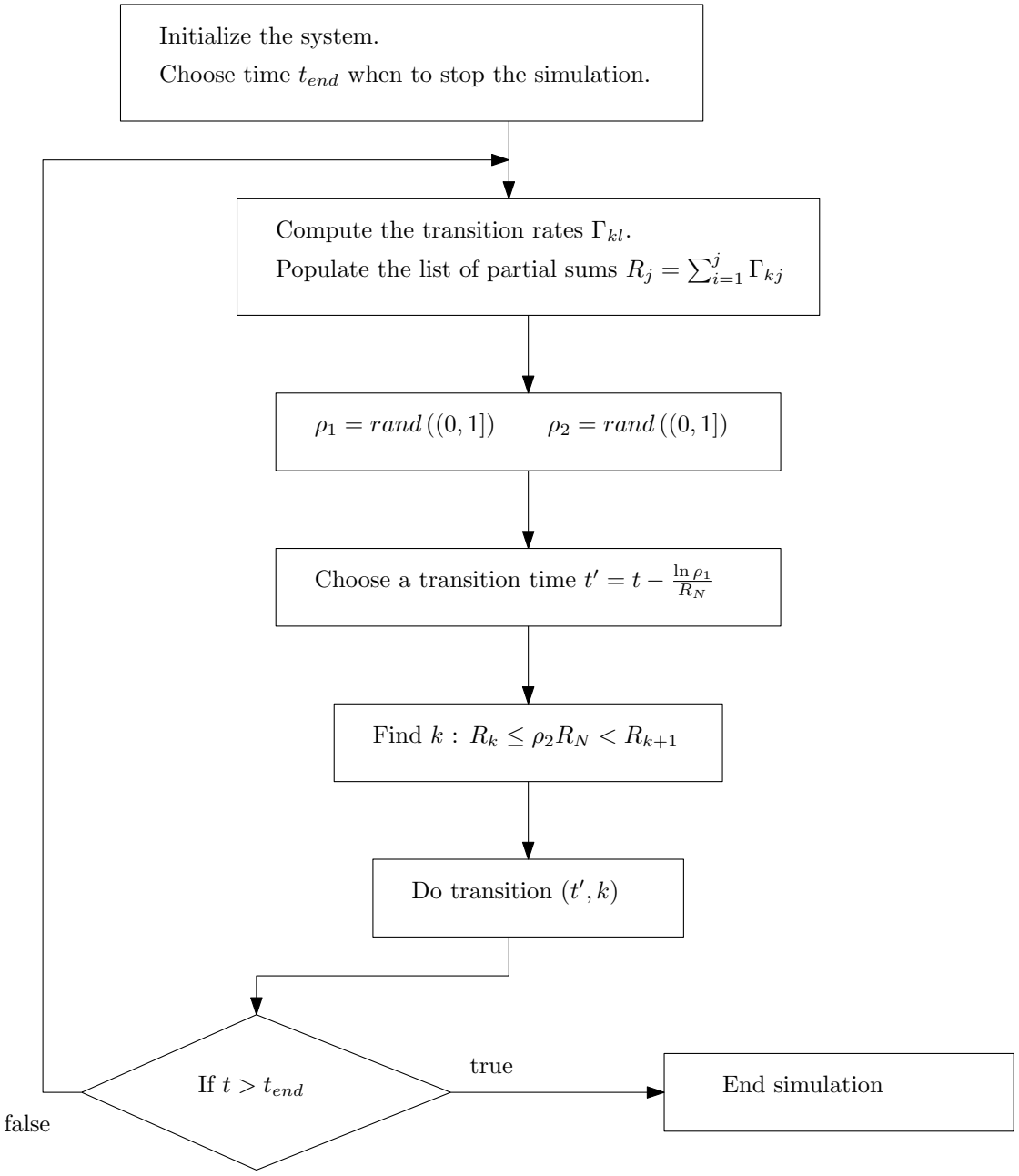

FIGURE 2.3. *Schematic structure of the NFW algorithm*

probability density $1 - p_{\text{survival}}(t')$ is itself a random variable with values in $(0, 1]$ and, as a consequence of that, the time step Δt is chosen to satisfy the equation

$$-\ln \rho_2 = \int_t^{t+\Delta t} R_N(\tau)\, d\tau \tag{2.5}$$

where ρ_2 is a random number in $(0, 1]$.

Having chosen the time $t' = t + \Delta t$ of the next transition the algorithm needs to chose what transition will be carried out. Just before the time t' the system is still in the state k. According to the master equation (2.1) the probability to find the system in the state l at time $t' + dt'$ is given by $\Gamma_{kl}(t')\, dt'$. The final state can be then chosen as shown in Figure 2.2 and in equation (2.2) using the rates, and their partial sums, computed at time t'. [24, 23]

2.1.2 Variants of the original NFW scheme

The N-Fold Way scheme is not the only possible formulation of a Kinetic Monte Carlo method. There are two notable variations of the original method: the First Reaction Time (FRT) and the Random Selection Method (RSM) algorithms. [19] All the methods reported here reproduce correctly the time evolution of the master equation (2.1).

Random Selection Method The RSM algorithm splits the choice of the transition in two different parts: the selection of the transition *type* and the selection of the *location* where the transition is to be applied. This method can be applied only in the case where the rates do not depend on time (i.e., $\Gamma_i(\tau) \equiv \Gamma_i$). The reaction time is chosen to be

$$\Delta t = -\frac{\ln \rho}{\max_i \Gamma_i} \tag{2.6}$$

where ρ is a random number uniformly chosen in $(0, 1]$ and i is an index that runs over all the types of transitions. The transition type and the location are picked randomly and, unlike in the NFW method, all the choices are equally probable. The time is updated at each step of the algorithm but the transition is applied with probability $\Gamma_i/\Gamma_{\max}$ only if the chosen type of transition is allowed on the location designed to be updated. The RSM

algorithm perform better when there is only one type of transition (or a very small number of them) having, in this case, complexity $O(1)$. However it cannot be applied to systems in which the rates depends on time, and so the RSM cannot be the method of choice in this thesis.

First Reaction Time The FRT method combines the selection of the reaction time and the selection of the transition in a single passage by choosing the first occurring reaction time t'_l from the set obtained solving the N equations

$$\int_t^{t'_l} \Gamma_{kl}(\tau)\, d\tau = -\ln \rho_l \qquad \forall l = 1 \dots N \tag{2.7}$$

where ρ_l are N random numbers in the interval $(0, 1]$. All the common implementations of this algorithm are very memory consuming but it generally performs better in terms of CPU time than the standard NFW approach when there is a strong dependence on time for the transition rates. See the reference [19] for more informations about this method.

2.2 Integration of the equations of motion

The equations of motion for a system with hamiltonian $\mathcal{H} = \mathcal{H}(\boldsymbol{q}, \boldsymbol{p}, t)$ are

$$\frac{d\boldsymbol{p}}{dt} = -\frac{\partial \mathcal{H}}{\partial \boldsymbol{q}} \tag{2.8}$$

$$\frac{d\boldsymbol{q}}{dt} = +\frac{\partial \mathcal{H}}{\partial \boldsymbol{p}} \tag{2.9}$$

and for a system of N classical particles interacting by means of a potential $V(\boldsymbol{q})$ in the three-dimensional space, these equations reduce to a set of $3N$ *Ordinary Differential Equations* (ODEs) of the second order.

2.2.1 Runge-Kutta methods

Consider a single ODE of the form

$$y'(x) = f(x, y) \tag{2.10}$$

with initial conditions $y(x_0) = y_0$. The basic idea to solve this equation for the unknown function $y(x)$ is to increment x by small amounts h and write, for each step

$$y(x+h) = y(x) + f(x, y(x))\, h. \tag{2.11}$$

This approach is known as *Euler's method* and it has very poor precision when compared with higher order algorithms, in fact the local truncation error, which is the error made in a single step of the algorithm, is proportional to h^2.

A modification of the Euler's method is the so called *midpoint method* in which the information on the value of the derivative in the middle of the step h is used to compute, with more precision, the function at the end of the interval. So one step of the midpoint method can be expressed as

$$y_{n+1} = y_n + h\, f\left(x_n + \frac{h}{2}, y_n + \frac{h}{2} f(x_n, y_n)\right) \tag{2.12}$$

where the notation $x_n = x_0 + nh$ and $y_{n+1} \equiv y(x_n)$ is introduced. The local truncation error for the midpoint algorithm is proportional to h^3 which makes it better than the Euler's method (for small h). In general a method with a local truncation error $O(h^{p+1})$ is said to be of pth order and so the Euler's method is a first order method while the midpoint method is a second order one.

Further development of this idea lead to the class of Runge-Kutta algorithms where each step can be formulated as

$$\begin{aligned} y_{n+1} &= y_n + h \sum_{j=1}^{s} b_j k'_{jn} \\ k'_{jn} &= f\left(x_n + c_j h, y_n + h \sum_{j=1}^{s} a_{ij} k'_{jn}\right) \end{aligned} \tag{2.13}$$

where s is the "number of stages" of the method, namely the number of evaluations k'_{jn} of the derivative inside the interval $[x_n, x_n + h]$ and the coefficients c_j, a_{ij} and b_j are specific of the particular method.

In the thesis this discussion is limited to *Explicit Runge-Kutta* methods that are methods

0				
c_2	a_{21}			
$\vdots$	$\vdots$	$\ddots$		
c_s	a_{s1}	$\dots$	$a_{s\,s-1}$	
	b_1	$\dots$	$\dots$	b_s

TABLE 2.1. *Butcher tableau*

0		
$1/2$	$1/2$	
	0	1

TABLE 2.2. *A 2-step Runge-Kutta algorithm of order 2*

for which the matrix of coefficients a_{ij} is lower triangular and has all zeroes on the diagonal.

$$a_{ij} = 0 \quad \forall i,j : j \geq i \implies \begin{bmatrix} 0 & \dots & \dots & 0 \\ a_{21} & \ddots & & \vdots \\ \vdots & \ddots & \ddots & \vdots \\ a_{s1} & \dots & a_{s\,s-1} & 0 \end{bmatrix} \tag{2.14}$$

Methods for which this statement is false are called implicit, and for them equations (2.13) are no longer linear (i.e., $y_{n+1} = y_n + f(x_{n+1}, y_{n+1})$). This nonlinear system has to be solved each time the solution needs to be advanced by a single timestep, adding a lot of computational work to the algorithm.

Different methods differ only in the choice of the coefficients, and they are often represented in a pictorial way in what is called a "Butcher's tableau" which is shown in the general case in Table 2.1 and in two real algorithms in Table 2.2 and in Table 2.3.

From Table 2.2 it is clear that for this particular choice of coefficient the Runge-Kutta algorithm reduce to the simpler midpoint rule (2.12).

0				
1/3	1/3			
2/3	−1/3	1		
1	1	−1	1	
	1/8	3/8	3/8	1/8

TABLE 2.3. *A 4-step Runge-Kutta algorithm of order 4*

2.2.2 Symplectic integrators

For a hamiltonian system whose $\mathcal{H}$ do not have explicit dependence upon time, the energy is conserved $\frac{d\mathcal{H}}{dt} = \frac{\partial \mathcal{H}}{\partial t} = 0$. When integrating the Hamilton equations (2.8) and (2.9) the solutions are required to

1. conserve the hamiltonian $\mathcal{H}(\boldsymbol{q}, \boldsymbol{p})$,

2. conserve the symplectic 2-form

$$\omega^2 = \sum_{i=1}^{N} dp_i \times dq_i \tag{2.15}$$

where the last requirement is a direct consequence of the fact that the flow in the phase space is volume-preserving. A method which satisfies these conditions is said to be *symplectic* [25]. The plot in Figure 2.4 shows the difference between a symplectic method (blue line) and a non-symplectic one (blue line) for a simple hamiltonian system.

A Runge-Kutta algorithm is symplectic only for a particular choice of coefficients that is

$$b_j a_{ij} + b_i a_{ji} - b_i b_j = 0 \quad \forall i, j \tag{2.16}$$

as pointed out in [26, p. 316]. An important consequence is that Explicit Runge-Kutta methods are never symplectic.

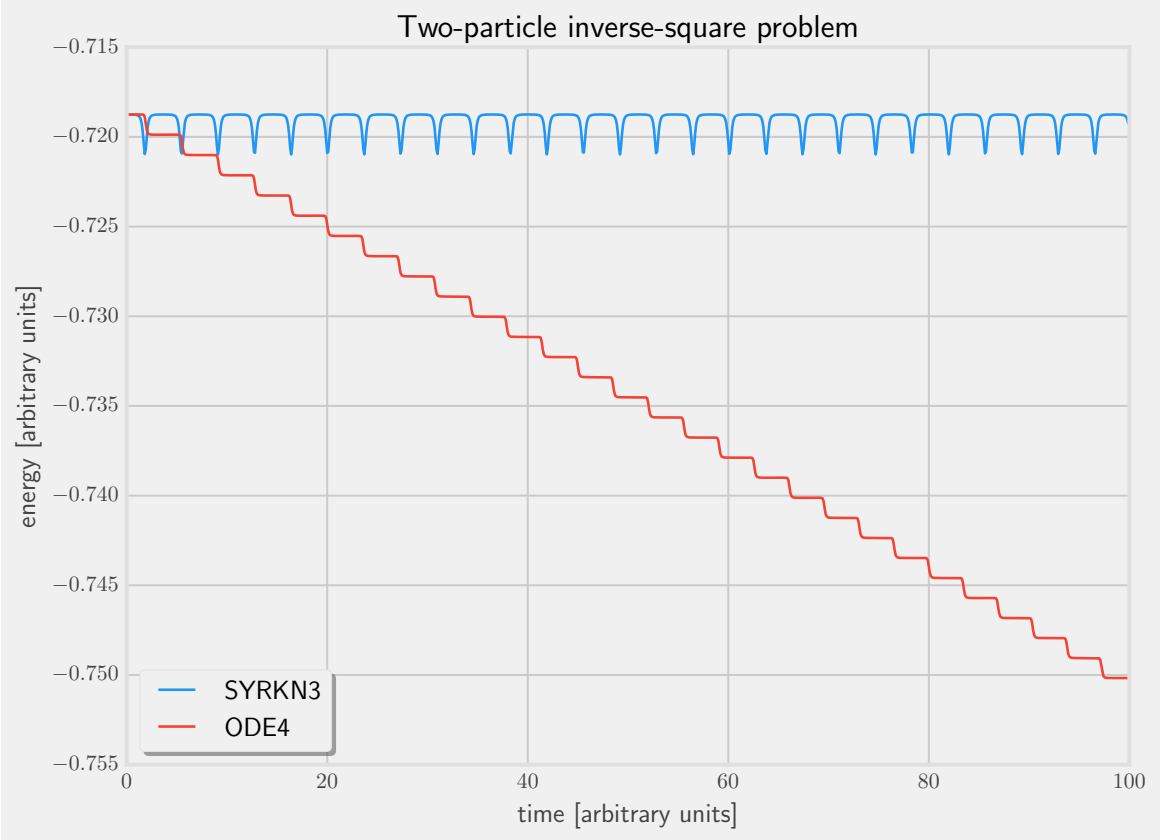

FIGURE 2.4. *Comparison of a non symplectic 4th order Runge-Kutta algorithm* ODE4 *with a symplectic algorithm of the same order* SYRKN3 *for the inverse-square problem where two particles repel each other with a force* $\propto 1/d^2$ *where* d *is the distance between the particles. The energy is plotted as a function of time.*

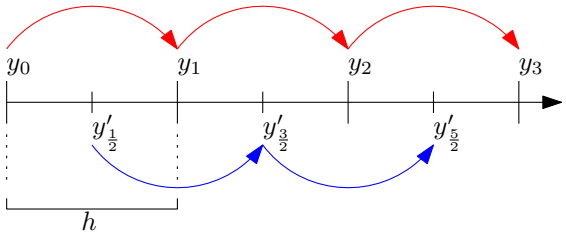

FIGURE 2.5. *Schematic representation of the leapfrog method. The functions and the first derivatives are computed at times* staggered *by* $h/2$.

2.2.3 Methods for separable Hamiltonians

While Explicit Runge-Kutta methods which are always symplectic (for a general, energy conserving hamiltonian) do not exists, this is not true in the very common case when the given Hamiltonian is separable and can be written as

$$\mathcal{H}(\boldsymbol{q}, \boldsymbol{p}) = T(\boldsymbol{p}) + V(\boldsymbol{q}) \tag{2.17}$$

with the kinetic energy in quadratic form $T(\boldsymbol{p}) = \sum_{i=1}^{N} \frac{p_i^2}{2m}$. For these systems the equations (2.8) (2.9) can be reduced to

$$\ddot{\boldsymbol{q}} = -\frac{1}{m}\frac{\partial V}{\partial \boldsymbol{q}} \tag{2.18}$$

which has the form $y'' = f(y)$. The fact that the equation (2.18) does not depend upon $\dot{q}$ can be used to simplify the integrator of the equations.

The leapfrog method A very basic *symplectic* method able to solve the equations (2.18) is the so called *Leapfrog* method. In this method the velocities (i.e., the first derivatives) are computed in the middle of the integration step h and then the velocities and the positions are advanced at staggered times. The basic step of the algorithm takes the form

$$y_{n+1} = y_n + h y'_{n+\frac{1}{2}} \qquad y'_{n+\frac{3}{2}} = y'_{n+\frac{1}{2}} + h \cdot f(y_{n+1}) \tag{2.19}$$

A schematic representation of this algorithm can be found in Figure 2.5.

The leapfrog method is of order 2 like the midpoint algorithm but unlike the latter, it evaluates the right hand side of the ODEs (the f function) only one single time for each

step, thus reducing drastically the amount of computational work required to advance the solutions for a single step. Even though it has a low precision, the leapfrog algorithm is widely used for solving Newton's equations of motion in molecular dynamics mainly because of its simplicity and speed.

Runge-Kutta-Nyström methods The Nyström methods are modifications of the standard Runge-Kutta method and are designed to take advantage of the form of the equation (2.18). For this type of systems there exist *symplectic* and *explicit* algorithms [26, p. 331] [27], whose basic step takes the form

$$\begin{aligned} y_{n+1} &= y_n + hy'_n + h^2 \sum_{i=1}^{s} b_i(i - c_i)k'_i \\ y'_{n+1} &= y'_n + h \sum_{i=1}^{s} b_i k'_i \\ k'_i &= f\left(y_n + c_i h y'_n + h^2 \sum_{j=1}^{i-1} b_j(c_i - c_j)k'_j\right) \end{aligned} \tag{2.20}$$

where the a_{ij} coefficient of the standard RK method are not needed anymore because $a_{ij} = b_j(c_i - c_j)$.

A 1-stage explicit RNK algorithm with coefficients $b_1 = 1$ and $c_1 = 1/2$ is equivalent to the *leapfrog* method and, like the latter, it is an algorithm of the second order.

In the present thesis a 3-stages explicit and symplectic method due to *Forest and Ruth* [28] is used. The algorithm is defined by the coefficients

$$\begin{aligned} c_1 = \frac{1}{2} - \gamma \qquad c_2 = \frac{1}{2} \qquad c_3 = \frac{1}{2} + \gamma \\ b_1 = \frac{1}{24\gamma^2} \qquad b_2 = 1 - \frac{1}{12\gamma^2} \qquad b_3 = \frac{1}{24\gamma^2} \end{aligned} \tag{2.21}$$

where γ is a zero of the polynomial $p(x) = 48x^3 - 24x^2 + 1$ which turns out to be [29] $\frac{1}{12}(2 - \sqrt[3]{4} - \sqrt[3]{16}) \approx -0.1756035959798288$. This method, here addressed as SYRKN3, is a *fourth order* Runge-Kutta-Nyström algorithm with only 3 stages, which means that the force in the right hand side of the equations (2.18) has to be computed only 3 times per step to obtain a local truncation error of order $O(h^5)$.

Higher order symplectic Runge-Kutta-Nyström algorithms exists in literature. In the reference [30] the authors develop an explicit method of order 8 while in [31] coefficient for implicit methods up to the 10th order are presented.

While it is clear why implicit methods are not considered in this thesis, the exclusion of higher order algorithms deserves an explanation. Consider a Hamiltonian system with N interacting particles. It is easy to see that, in the worst case, the computation of the force on a single particle has complexity $O(N)$ and the time required to compute all the forces acting on all the particles of the system is of order $O(N^2)$. The number of stages, which is the number of times the force is computed, is relevant, in terms of computational work, when the number of particles is high. The right balance must be found between the requirement of high performance (i.e., the leapfrog method) and the need for high numerical precision (i.e., 8th-order algorithms and beyond). In the present thesis SYRKN3 algorithm represents the optimal balance between performance and precision for integrating the equations (2.18).

2.3 Simulating both internal and external dynamics

While Kinetic Monte Carlo methods can be used to solve the internal dynamics of the toy model presented in the previous chapter, Runge-Kutta-Nyström methods can be used to solve the classical equations of motion (2.18) to gain the time evolution of the external degrees of freedom, namely the motion of the particles.

These two methods can be combined to work together to resolve the dynamics of both external and internal degrees of freedom. This is done by modifying the step of the KMC algorithm when the time of each reaction is chosen. The transition rates of the system will depend on time, and their evolution obtained by solving the equation of motion with the SYRKN3 algorithm between two transitions. The value of the integral on the right hand side of equation (2.5) is computed step by step, and when it reaches the randomly chosen value on the left hand side the transition time t' is found. Then the KMC algorithm is applied using the rates computed at t' to choose the transition.

Multiple steps of this algorithm will result in the exact (statistical) solution of the master equation (2.1).

Chapter 3

Nonequilibrium dynamics of a many-body system

The theory and methods developed in the preceding two chapters are used, in the present one, to study the excitation dynamics out of equilibrium for a system of strongly interacting Rydberg atoms. A Kinetic Monte Carlo method is used to solve the time evolution of the studied systems under different conditions and for different regimes of the excitation process. The main interest here is to study how the phenomena of the facilitation and the blockade affect the dynamics out of equilibrium and how these effects can be used to control the internal state of the system.

The chapter is structured as follows. First the results of different simulations upon regular and ordered systems are presented. The resonant and off-resonant dynamics of these systems is studied. A time-dependence of the excitation parameters is then introduced in the shape of a quench (sudden change) in the detuning. Finally, a variable amount of disorder in the positions of the atomis is introduced in order to allow a better comparison with experiment.

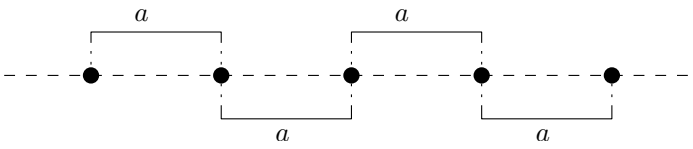

FIGURE 3.1. *Schematic of the ordered system studied.*

3.1 Dynamics of a $R_b/2$ chain

The system we want to study in this chapter is a regular one-dimensional lattice (a *chain*) with spacing a as seen in Figure 3.1, where the atoms are fixed to the lattice sites.

As explained in Chapter 1 the transition rates for the atoms of this system are given by

$$\Gamma_k = \frac{\Omega^2}{\gamma} \frac{1}{1 + \frac{1}{\gamma^2}(\delta - V_k)^2} \tag{3.1}$$

where, referred to the transition from the ground state to the Rydberg states, Ω indicates the Rabi frequency, γ the linewidth of the laser used, δ the detuning and $V_k = \sum_{m \neq k} \frac{C_\alpha}{|r_m - r_k|^\alpha}$ is the total interaction potential at the site k. The blockade radius, defined as the distance from an already excited atom for which, at resonance, where $\delta = 0$, the rate is half its maximum value, is given by

$$R_b = \left(\frac{C_\alpha}{\gamma}\right)^{\frac{1}{\alpha}} \tag{3.2}$$

while, off resonance, when $\delta \neq 0$, the facilitation radius is

$$r_{\text{fac}} = \left(\frac{C_\alpha}{\delta}\right)^{\frac{1}{\alpha}} \tag{3.3}$$

and is defined as the distance from another excitation where the rate Γ is maximum.

The simulations presented in the present chapter refer to $1D$ lattices with spacing $a = R_b/2$. This choice has been made because the facilitation radius is always $r_{\text{fac}} < R_b$ and this is a constraint for the study of the effect of facilitation in the off-resonant dynamics. Then, regarding systems with this particular spacing and given the definitions (3.2) and (3.3) three different and intresting regimes are accessible to study:

- on resonance, where $\delta = 0$;

- off resonance with $\delta = 2^{\alpha}\gamma$;
- again off resonance but with $\delta = 2^{\alpha+1}\gamma$.

The *resonant excitation* of the system is interesting because here the blockade is expected to have non trivial effects to the dynamics approaching the equilibrium as can be seen in the paper by *Lesanovsky* [10] (the corresponding case in that paper is for $R = 2 \Rightarrow a = R_b/2$). Consider the presence of a single excitation on the lattice while the chain is being excited on resonance. Its nearest neighbors, which are at distance $R_b/2$, have strongly suppressed excitation rates

$$\Gamma\left(\frac{R_b}{2}\right) = \frac{\Omega^2}{\gamma}\frac{1}{1+2^{2\alpha}} \ll \Gamma(r \to \infty) \tag{3.4}$$

while the rate on the second-nearest neighbors is $\Gamma(R_b) = \frac{\Gamma(r\to\infty)}{2}$ and finally from the third nearest neighbor to the farthest atom in the lattice $\Gamma \simeq \Gamma(r \to \infty)$. This means that when some atoms in the chain are already excited the excitation of the others is very unlikely which leads to a slowing down of the dynamics while approaching the equilibrium.

Atoms whose transitions (both excitations and de-excitations) are forbidden or very unlikely on the timescale of the simulation because $\Gamma \approx 0$ will be called *frozen*.

The *off-resonant case with* $\delta = 2^{\alpha}\gamma$ has been chosen because this is the detuning for which the lattice parameter $a = R_b/2$ is exactly the facilitation radius (3.3). So in this regime we expect to observe a speedup of the dynamics due to the facilitation effect when some excitations are already present in the system.

The choice of the last regime, *off-resonance with* $\delta = 2^{\alpha+1}\gamma$, is the least intuitive of the three. Consider a plaquette composed of three atoms on three adjacent sites of the lattice. If the two atoms at the extremes of the plaquette are excited, the potential at the middle one, which is at a distance $R_b/2$ from the other two, is $2^{\alpha+1}\gamma$. So with the choosen detuning, the excitation or de-excitation of this atom will be facilitated because $\delta - V = 0$ and so the transition rate of the atom in the middle is $\Gamma_{\text{middle}} = \Gamma_{\text{max}}$.

In order to facilitate the comparison with the experiments performed in the laboratory, the simulations presented in this chapter are done for a specific choice of parameters. First of

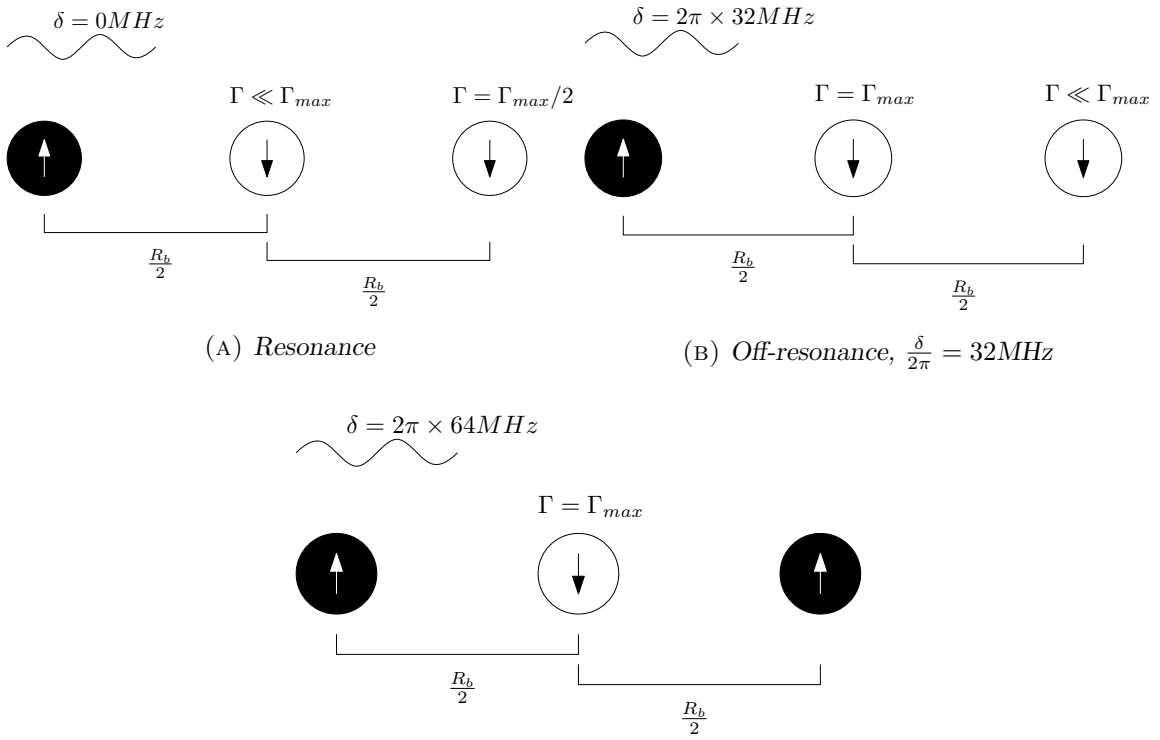

(A) *Resonance*

(B) *Off-resonance,* $\frac{\delta}{2\pi} = 32MHz$

(C) *Off-resonance,* $\frac{\delta}{2\pi} = 64MHz$

FIGURE 3.2. *Three different schemes of excitations for a chain whose distance parameter is equal to* $R_b/2$

all, Rydberg atoms (as will be shown in the next chapter) interact by means of a potential C_6/r^6 and so $\alpha = 6$ [32, 33] will be used in the simulations. The Rabi frequency will be taken to be $\frac{\Omega}{2\pi} = 1.0\,\text{MHz}$ while the linewidth of the radiation is taken to be $\frac{\gamma}{2\pi} = 0.5\,\text{MHz}$ according to the values commonly used in the experiments performed in Pisa.

Using these parameters the two chosen detunings become

$$\delta = 2^{\alpha}\gamma \quad \Longrightarrow 2\pi \times 32\,\text{MHz} \tag{3.5}$$

$$\delta = 2^{\alpha+1}\gamma \Longrightarrow 2\pi \times 64\,\text{MHz} \tag{3.6}$$

Figure 3.2 shows a schematic representation of what is to be expected in each of these three regimes in the conditions specified above.

3.1.1 Dynamics at resonance

Our discussion of the dynamics at resonance is based on the reference [10]. The case discussed here, a $1D$ lattice with spacing $R_b/2$ corresponds to the case $R = 2$ discussed in that paper, where $R = \frac{1}{a}\left(\frac{C_\alpha}{\gamma}\right)^{1/\alpha}$ is the number of atoms inside a single blockade radius.

Our results are presented in Figure 3.3 and corresponds to averages over 100 different shots over a system of 100 atoms starting from the ground state $|\downarrow\downarrow\downarrow\cdots\rangle$. The mean number of excitations (averaged on all the shots) which is the population of the state $|\uparrow\rangle$ is plotted as a function of time.

As can be seen in Figure 3.3 the population of the Rydberg state reaches the stationary value of 50 excitations after $10^4\mu$s, but the dynamics approaching this value is not trivial. The main feature of these results is the plateau present at about 30 excitations which spans the times from 1μs to 100μs and represents a dramatic slowing down of the dynamics on resonance.

The value at which this plateau appear is predicted in the reference [10] by mean field solution of the effective master equation (1.8) and correspond to a density of excited atoms

$$\frac{N_e}{N} = \rho_{\text{plateau}} = \frac{1}{2}\left(1 - \frac{1}{\sqrt{5}}\right) \approx 0.276 \tag{3.7}$$

(see [34]).

This plateau is a consequence of the fact that simultaneous excitation of neighboring spins is strongly suppressed because of the blockade effect and, following the discussion in the paper, the system is in a mixed state of all configurations where no nearest neighboring atoms are excited. The mean density of these states is just the one reported in equation (3.7).

This effect can be better understood considering the two possible states of the system pictured in Figure 3.4. The state (a) is a possible state in correspondence of the plateau. In this state all the atoms in the ground state have low excitation rates compared to the de-excitation rates of the already excited atoms. To reach a configuration similar to the one pictured in the part (b) of the Figure 3.4, the system needs to rearrange itself by de-

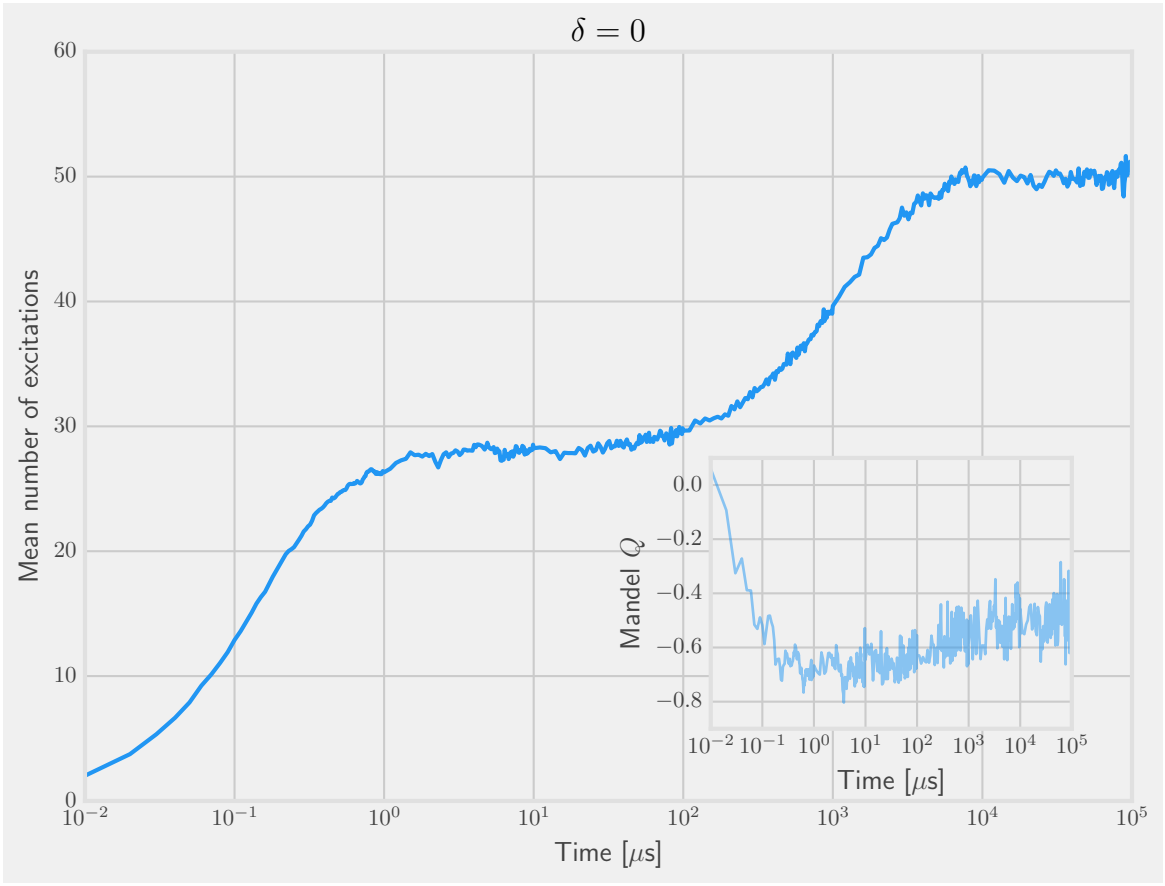

FIGURE 3.3. *The excitation of a chain of 100 atoms with distance parameter $R_b/2$ starting at $t = 0$ from its ground state. The mean number of excitations, averaging over 100 realizations of the simulation, is plotted as a function of the time.*

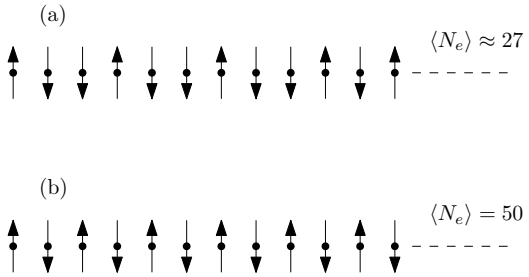

FIGURE 3.4. *Schematic representation of two different states of the system. The state in the part (a) of the figure is a possible state in correspondence of the plateau while the state in the part (b) is a sample state for the stationary value of the number of excitations.*

excitations and successive excitations. In this phase of the evolution of the system there is no net change in the number of excitations, leading to the plateau observed in Figure 3.3.

In the inset in Figure 3.3 the so called Mandel's Q-parameter [35] is plotted as a function of time for the resonant excitation process. The Q-parameter is defined by

$$Q = \frac{\langle N_e^2 \rangle - \langle N_e \rangle^2}{\langle N_e \rangle} - 1 \tag{3.8}$$

where N_e is the number of excitation and $\langle \cdots \rangle$ denotes the average over the probability distribution. This parameter measures the deviation of the probability distribution from a *Poissonian* distribution for which $Q = 0$. For super-poissonian distributions the Q-parameter is positive while for sub-poissonian distribution it is negative. We have found that in order to obtain good statistic to compute stable values of the Mandel Q-parameter we need to repeat the simulations around 100 times. To obtain reasonable computing time we have limited the size of the system to 100 atoms.

Intuitively consider the case of a chain where the spacing is $a \gg R_b$ so that the interaction among the atoms are negligible. In this case, the excitation of one atom is independent from the excitation of the others and, given the master equation (1.8) the process is Poissonian so $Q = 0$. As we can see from the inset in Figure 3.3, when the system is in its ground state at $t \approx 0$, there is no interaction among the atoms and hence $Q \approx 0$. Because for

the system used the spacing is $a < R_b$ the interaction are no negligible and so when some excitations begin to show the Q decreases. This is a consequence of the blockade effect which results in the *anticorrelation* of the excitation processes (the probability of having n excitation decrease with the increase of the probability of having $n-1$ excitations).

3.1.2 Off-resonant dynamics

Our results of simulations in the case of off-resonant dynamics are reported in Figure 3.5. Here the mean number of excitations for the two different off-resonant regimes with detunings 32 MHz (red line) and 64 MHz (blue line) is plotted as a function of time. For comparison the time evolution of the Rydberg states on resonance is also reported (purple line).

For the first ten micro seconds in the case of $\frac{\delta}{2\pi} = 32\,\text{MHz}$ and for the first 100μs in the case at 64 MHz, there is no excitation. This is a noticeable slowing down with respect to the case at resonance which at the same times presents on average ≈ 27 excitations. This is due to the fact that, when the system is in its ground state $|\downarrow\downarrow\downarrow\cdots\rangle$ the transition rate of all the atoms is given by

$$\Gamma = \frac{\Omega^2\gamma}{\gamma^2+\delta^2} \tag{3.9}$$

and so, in both the off resonant regimes the creation of excitations is heavily suppressed by a factor $\frac{\gamma^2}{\gamma^2+\delta^2}$ with respect to the resonant case which is equal to 6.1×10^{-5} in for the case at 64MHz and 2.4×10^{-4} for the case at 32MHz.

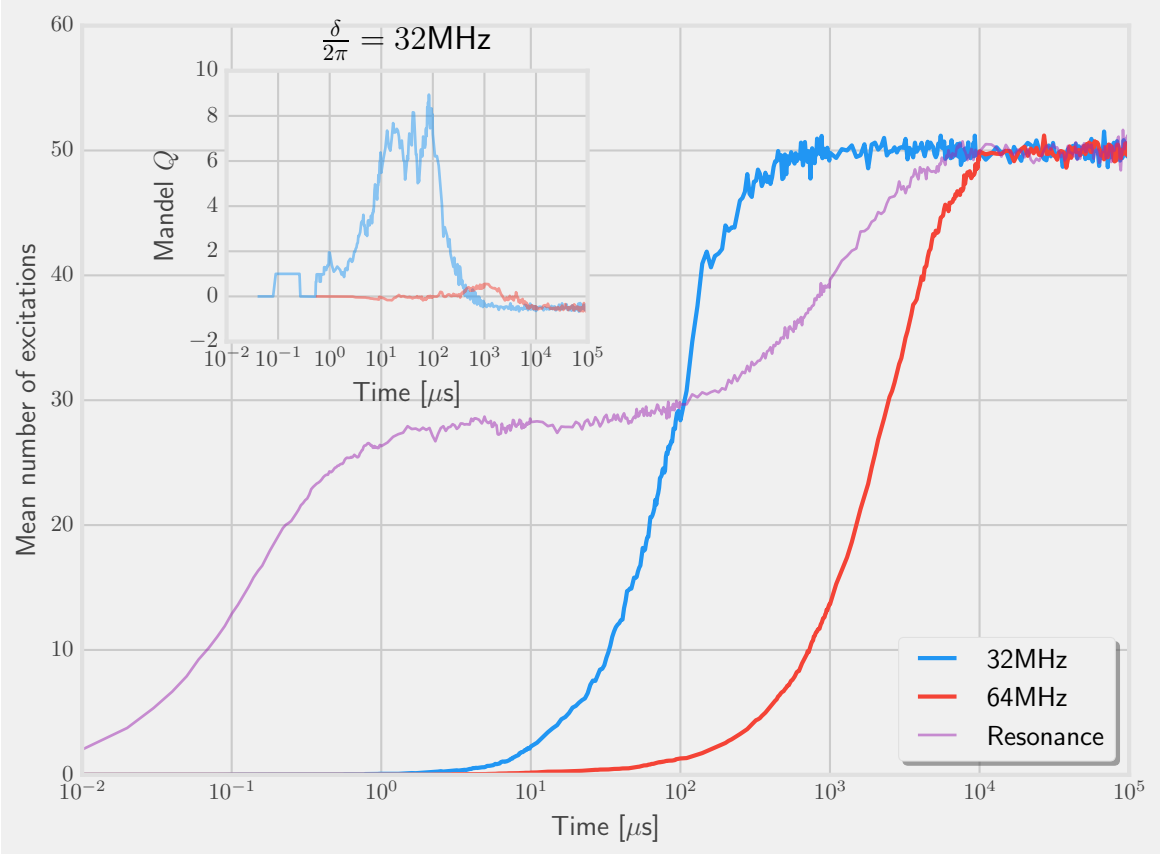

FIGURE 3.5. *Off-resonant excitation of a chain of 100 atoms with distance parameter $R_b/2$ starting at $t = 0$ from its ground state. The excitation is presented for different values of the detuning: $\frac{\delta}{2\pi} = 32MHz$ (blue line) and $\frac{\delta}{2\pi} = 64MHz$ (red line) and conpared to the resonant excitation (purple line) which is the same as Figure 3.3. The mean number of excitations, obtained by averaging over 100 realizations of the simulation, is plotted as a function of the time. In the inset the Mandel's Q-parameter is plotted as a function of time for the case $\frac{\delta}{2\pi} = 32MHz$.*

After $10^3 - 10^4 \mu$s the population of the Rydberg state reaches the stationary value $\approx 50\%$ as in the resonant case but the interesting feature shows up at mid-range times. Here the excitation process is much faster at populating the excited level than in resonant excitation. This effect is a consequence of the facilitated dynamics. Take for example the case of $\frac{\delta}{2\pi} = 32MHz$ reported in Figure 3.2b. When a single excitation is already present on the lattice the rates of its first neighbors will be maximum while the rates of all the other atoms will be almost zero. So the nearest neighbors of the original excitation are very likely to be excited. As soon as that excitation occurs all its neighbors will now be facilitated and so on, starting a *chain process* (avalanche) which not only speeds up the excitation process and the approach to the stationary value, but also leads to the creation of *clusters*, namely groups of Rydberg atoms which occupy adjacent sites of the lattice. [36]

These chain processes are an example of *correlated processes* in the sense that consequent excitations depend on each other (i.e., the probability of having n excitations increase with the probability of having $n-1$ excitations). This the exact opposite of what described in Section 3.1.1 for the dynamics at resonance.

In the inset in Figure 3.5 the Mandel's Q is plotted as a function of time for the case of $\frac{\delta}{2\pi} = 32\,\text{MHz}$ (blue line). So for the time scales in which the *chain process* is expected to happen, the Q-parameter is $Q > 0$ while being $Q \leq 0$ for initial times and when the system has reached the stationary value for $\langle N_e \rangle$. The effect is less visible in the case $\frac{\delta}{2\pi} = 64\,\text{MHz}$ (red line) because the number of correlated excitations that may happen in the system are less than in the case at 32 MHz.

3.1.3 Quenches in detuning: from resonant to off resonant dynamics

A very clean setting for non-equilibrium dynamics is the one emerging from a sudden global quench (which for our systems could be a sudden change in detuning). In these situations questions arise on how the system continues its time evolution under the new conditions and how the time scales for equilibration are altered after the quench.

In Figure 3.6 we present some results for quenches in the detuning from resonance to 32MHz (as seen in Figure 3.6a) and from resonance to 64MHz (Figure 3.6b). These quenches are done after 10μs of resonant excitation which correspond to the timescales in which the system is at the plateau $\langle N_e \rangle \approx 27.6$.

As mentioned before, in correspondence of this plateau the system is in a mixed state of all configurations where no nearest neighboring excitations exists. So switching from this regime to $\frac{\delta}{2\pi} = 32\,\text{MHz}$ where the excitation of the nearest neighbors of an atom in the Rydberg state is facilitated, is expected to result in a speed up of the dynamics.

For the quench $\delta = 0 \rightarrow \frac{\delta}{2\pi} = 64MHz$ the number of atoms which have facilitated dynamics just after the switch is expected to be lower then in the previous case. Considering the part (a) of the Figure 3.4 it can be seen that the atoms having both their nearest neighbors excited are less in number than the atoms having only one nearest neighbor excitation and so the speed up of the dynamics will be less evident in this case.

From the data presented in Figure 3.6 all the features just discussed are visible. In particular is to be observed the difference in the magnitude of the effect of the two different quenches.

3.1.4 Dynamics from an ordered state

In Sections 3.1.1, 3.1.2 and 3.1.3 we have performed simulations of the out of equilibrium dynamics for a chain with spacing $R_b/2$ starting from the ground state of the chain. Now we want to study the dynamics from an artificially chosen state different from the ground state. An example would be the ordered state

$$|\uparrow\downarrow\uparrow\downarrow\cdots\downarrow\uparrow\downarrow\cdots\rangle \tag{3.10}$$

which has $\langle N_e \rangle = 50$ as in the stationary state.

Results from simulation of the dynamics are presented in Figure 3.7 and show unexpected results for the resonant case and for the off-resonant one with $\frac{\delta}{2\pi} = 64\,\text{MHz}$.

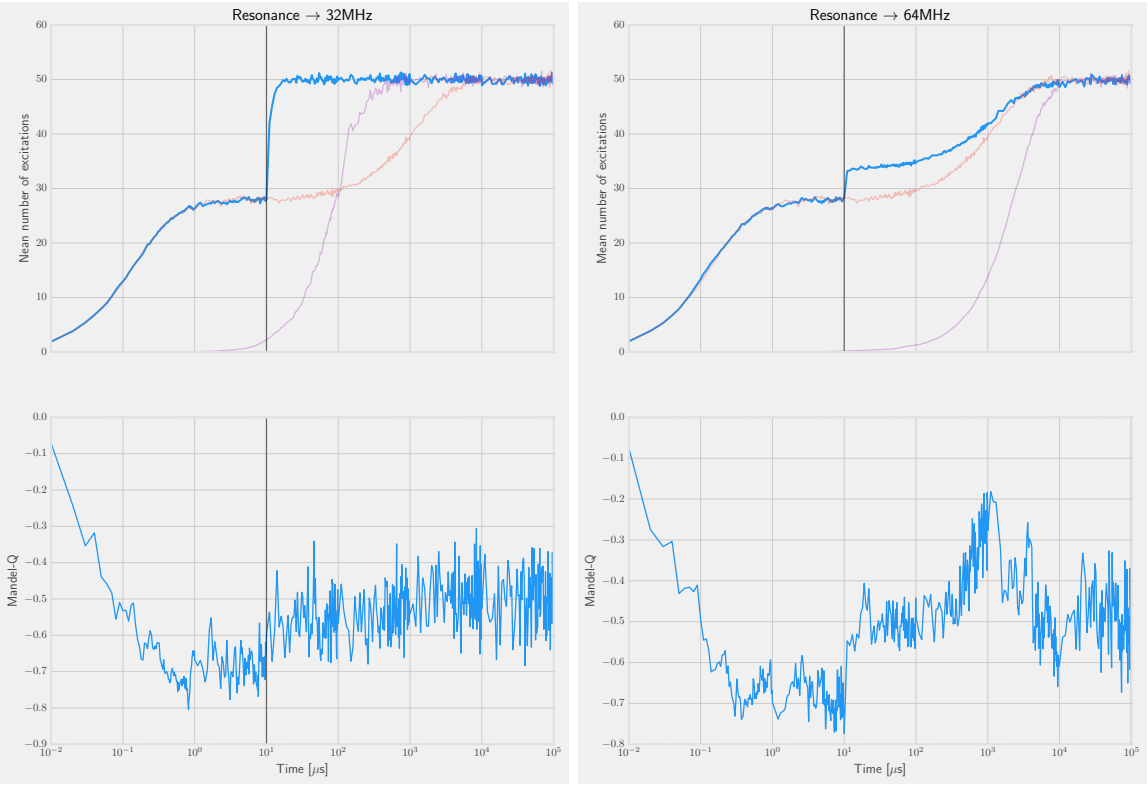

(A) *Switch* $0.0 \rightarrow 32MHz$. (B) *Switch* $0.0 \rightarrow 64MHz$.

FIGURE 3.6. *Results of simulations with switches to off-resonant dynamics from resonance for a chain of 100 atoms and distance parameter* $R_b/2$ *The quenches of the detunings are* $0.0 \rightarrow 32MHz$ *and* $0.0 \rightarrow 64MHz$ *and are performed at a time* $t = 10\mu s$ *when about* $1/3$ *of the atoms are excited. In the upper part of each graph the mean number of excitations, obtained by averaging over 100 repetitions of the simulation, is plotted as a function of time. In the lower part the time evolution of the Mandel-Q parameter is presented.*

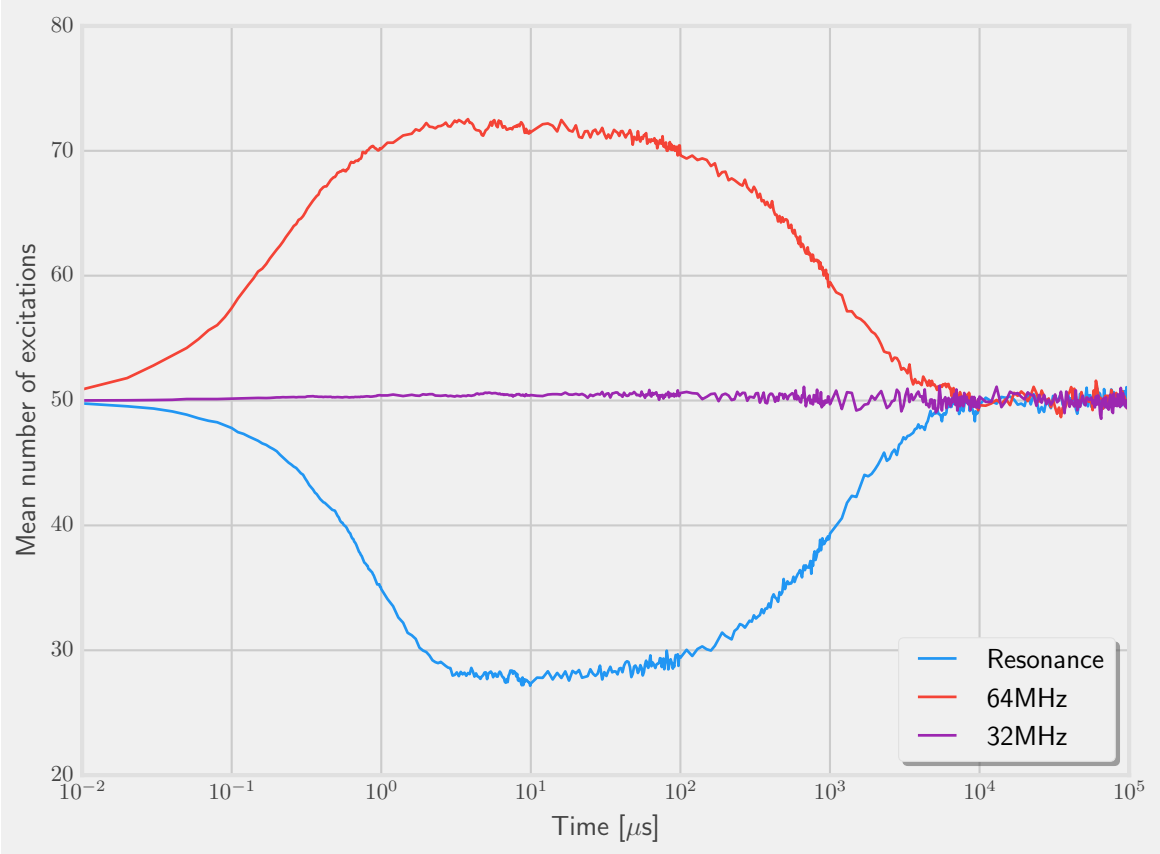

FIGURE 3.7. *The mean number of excitations (over 100 samples) is plotted as a function of the excitation time for the cases of resonant dynamics (blue line), and off-resonant with detunings 32MHz (red line) and 64MHz (purple line) for a system of 100 atoms at distance $R_b/2$ and starting from the ordered state* $|\uparrow\downarrow\uparrow\downarrow\uparrow\cdots\rangle$

While the system when excited at 32 MHz seems to be in its stationary state and no variations from this state are observed, for the other two cases the dynamics approaching $\langle N_e \rangle \approx 50$ is non trivial.

In the off-resonant case with $\frac{\delta}{2\pi} = 64\,\text{MHz}$ (red line) all the atoms initially in the state $|\downarrow\rangle$ are facilitated as they have two excited neighbors (see Figure 3.2c) while in the resonant case excitation of these atoms is strongly suppressed. The de-excitation rates of the already excited atoms are $\Gamma_{\max}/2$. This explains why initially the mean number of excited atoms grows for the case at 64MHz and decreases for the resonant case. Then for the resonant case the same plateau presented in Figure 3.3 is reached (≈ 27.6 excitations) and from there the system continues its dynamics towards the stationary state.

Another unexpected effect manifests itself in the case of the off-resonant dynamics at 64MHz of detuning. Here a plateau is reached at the value $\approx N(1 - 0.27)$ where N is the total number of atoms in the system. The two different plateaus, the one from the resonant excitation and the other from the case of detuning at 64MHz appears at symmetric values with respect to the value $\langle N_e \rangle = 50$. In this case most of the atoms are excited and, basing our discussion on [10] a simple explanation of this effect can be given As discussed in Section 3.1.1, on the plateau appearing in the resonant dynamics the system is in a mixed state of all configurations where no neighboring excitations exists. The same situation arises in the case with $\frac{\delta}{2\pi} = 64\,\text{MHz}$ where no neighboring atoms in the ground state exists and the de excitation of already excited atoms is suppressed. The system has to rearrange itself to continue its evolution towards its stationary state and this rearrangement implies no net change of the number of excitations which leads to the plateau observed in Figure 3.7 for the off-resonant excitation process with $\frac{\delta}{2\pi} = 64\,\text{MHz}$.

3.2 Studying the effects of the disorder

The studies presented so far were carried in an ordered system and are useful in that they allow us to understand what kind of phenomena to expect. Some experiments can realize

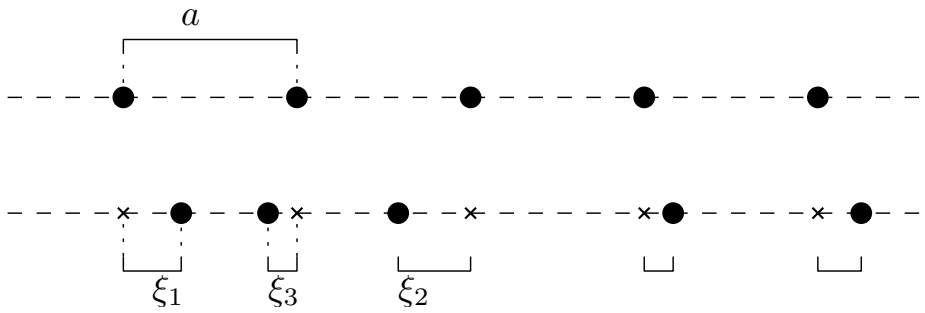

FIGURE 3.8. *Schematic representation of the disordered system used. each atom is displaced from the regular lattice site by a distance ξ chosen randomly in the interval* $[-\phi\frac{a}{2}, \phi\frac{a}{2}]$

such ordered systems [37, 38] thanks to various techniques of trapping of the atoms, but most experiments, like the one in Pisa, use disordered atomic gasses. It is important, therefore, to understand which of these effects survive with the introduction of some kind of disorder in the system.

The system which will be studied in this section is represented in Figure 3.8. Starting from the case of a regular one-dimensional lattice a small displacement ϕ is added moving each atom from in lattice site by a random quantity $\xi \in [-a \cdot \phi, a \cdot \phi]$ where a is the spacing of the regular lattice.

Results for excitation on resonance for different values of ϕ are presented in Figure 3.9 where different values of ϕ are tested on a system with spacing $a = R_b/2$.

In the first micro second of the excitation process, the time evolution of the mean number of excitation is the same for all the different values of ϕ. This is compatible with the creation of distant and uncorrelated excitations which aren't affected by the added disorder.

Then, as can be seen from Figure 3.9, the plateau observed characteristic for the ordered system gradually disappears when the disorder is added to the system. Also, an increase of the disorder parameter ϕ results in an increase in the time at which the system reaches its stationary value.

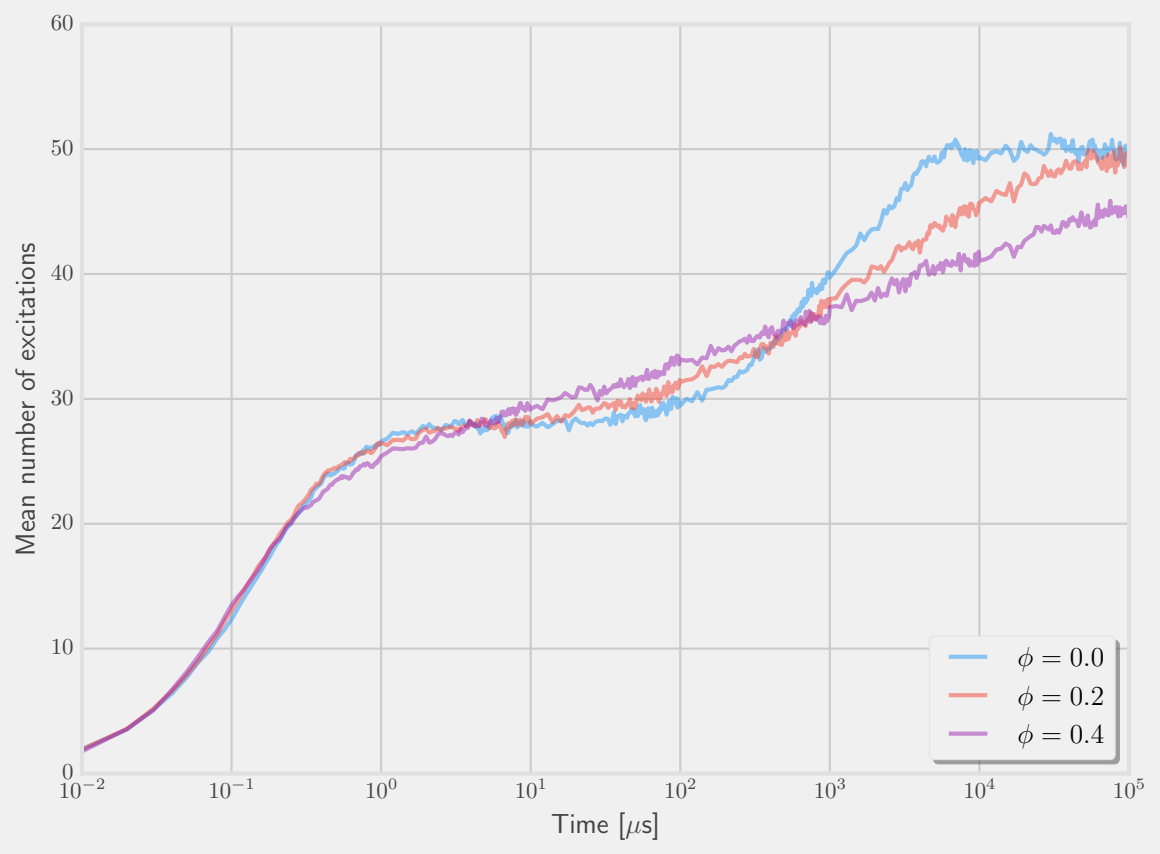

FIGURE 3.9. *The mean number of excitation for a disordered chain of 100 atoms is plotted as a function of time for different values of the ϕ parameter.*

3.3 Conclusions

We have seen in this chapter how the blockade and the facilitation affects the dynamics of the internal degrees of freedom of a one-dimensional lattice. We have studied the time evolution of the system in different conditions and at different regimes. Studying a chain with spacing $a = R_b/2$ on resonance we found a dramatic slowing down of the dynamics when the number of excitations is about $1/3$ of the total number of atoms in the system. Following the discussion in [10] we are able to identify the causes of this slowing down to the blockade effect.

Our study of the off-resonant excitation process evidenced a fast and strongly correlated dynamics for appropriate choices of the detuning. We found that, due to the facilitated dynamics of atoms at distance r_{fac} from an excitation, fast consecutive excitation could result in an avalanche process that ultimately causes the speedup of the dynamics.

Then we tested the response of the system to sudden changes in the detuning and found that when switching from on resonant excitation to the off-resonant one the system reaches faster the stationary state evidencing the effects of the facilitation.

The dynamics approaching the equilibrium from an ordered state different from the ground state has evidenced unexpected behaviours of the system showing a dramatic slowing down, similar to the one found in the dynamics at resonance, for the off-resonant excitation process with $\delta = 2^{alpha+1}\gamma$ ($2\pi \times 64\,\text{MHz}$ with our choice of parameters).

Finally we studied the effect of added disorder to the system in order to understand which of the features discovered in the ordered case can be observed in experiments, like the one in Pisa, which uses disordered gasses of Rydberg atoms.

Chapter 4

Van der Waals interaction

With the term *van der Waals forces* are indicated all the interactions between atoms, molecules and surfaces caused by correlations in the fluctuating polarizations of nearby particles; these interactions include [39]:

- the force between permanent dipoles, known as *Keesom force*;
- the force between a permanent dipole and an induced one, known as *Debye force*;
- the force between two induced dipoles, known as *London dispersion force*

The origin of the term comes from Johannes Diderik van der Waals who introduced for the first time these forces in his PhD. thesis [40] in 1873 as a correction to the interaction between particles in the state equation of perfect gasses.

The van der Waals interaction between Rydberg atoms has been measured using spectroscopic tecniques [41, 42]. Also the interactions between Rydberg atoms and metal [43, 44, 45] or dielectric surfaces [46] has been studied.

In this chapter the theory of van der Waals interaction between Rydberg atoms is introduced. Numerical studies of the coupled dynamics of external and internal degrees of freedom of interacting Rydberg atoms are presented. Finally a method to directly observe the van der Waals interaction between Rydberg atoms is presented along with the experimental and

numerical results obtained in the experimental cold atoms group in Pisa [47].

4.1 Dipole-dipole and van der Waals interaction

The dipolar or van der Waals interactions between two neutral but polarizable atoms can be introduced in a general way considering the simple model of two hydrogen-like atoms with only one electron in the outermost shell. The interaction Hamiltonian between the two atoms A and B that lie a distance R apart along the direction $\boldsymbol{n}$ is given by

$$H_{\text{int}} = \frac{e^2}{4\pi\epsilon_0}\left(\frac{1}{R} - \frac{1}{r_{A1}} - \frac{1}{r_{B2}} + \frac{1}{r_{12}}\right). \tag{4.1}$$

Using the relation $\left(|\boldsymbol{R}+\boldsymbol{r}|^2\right)^{\frac{1}{2}} = \frac{1}{R}\left(1 - \frac{\boldsymbol{n}\cdot\boldsymbol{r}}{R} - \frac{3(\boldsymbol{n}\cdot\boldsymbol{r})-\boldsymbol{r}}{2R^2} + \dots\right)$ the leading term of the expansion of the Hamiltonian at large distances R is called the dipole-dipole operator and takes the form

$$V_{dd} = \frac{\boldsymbol{\mu}_1\cdot\boldsymbol{\mu}_2 - 3(\boldsymbol{n}\cdot\boldsymbol{\mu}_1)\cdot(\boldsymbol{n}\cdot\boldsymbol{\mu}_3)}{4\pi\epsilon_0 R^3} \tag{4.2}$$

with $\boldsymbol{\mu}_1$ and $\boldsymbol{\mu}_2$ the dipole moments of each atom. Because the interatomic distance R is taken to be large with respect to the distances between the electrons and their respective atomic nuclei, the exchange interaction between the two electrons can be neglected and so there is no confusion in the notation $\boldsymbol{\mu}_1$ and $\boldsymbol{\mu}_2$.

Now suppose that the two atoms are in the initial states $|r_1\rangle_A$ and $|r_2\rangle_B$. The dipole-dipole interaction causes the transition between the state $|r_1, r_2\rangle = |r_1\rangle_A |r_2\rangle_B$ and the pair state $|r_1', r_2'\rangle$ with an energy difference between the final and initial two-atom state

$$\hbar\Delta = E_{|r_1', r_2'\rangle} - E_{|r_1, r_2\rangle} \tag{4.3}$$

called Förster defect. In the atomic base $\{|r_1', r_2'\rangle, |r_1, r_2\rangle\}$ the interaction Hamiltonian can be written

$$H_{\text{int}} = \begin{pmatrix} \hbar\Delta & V \\ V^\dagger & 0 \end{pmatrix} \tag{4.4}$$

where the off-diagonal term is $V = \langle r_1, r_2 | V_{dd} | r_1', r_2' \rangle$ which can be written as C_3/R^3 by direct substitution of (4.2). Diagonalization of this matrix gives the eigenenergies

$$E_\pm = \frac{1}{2}\left(\hbar\Delta \pm \sqrt{(\hbar\Delta)^2 + 4V^2}\right) \tag{4.5}$$

for the new eigenstates $|\tilde{r}_1, \tilde{r}_2\rangle$ and $|\tilde{r}_1', \tilde{r}_2'\rangle$.

Here two different regimes can be recognized.

- $\hbar\Delta \ll V$. This is the case of nearly degenerate eigenstates, and the eigenenergies are given by $E_\pm \approx \pm V$. This results in resonant $\frac{C_3}{R^3}$-dipole-dipole interaction.
- $\hbar\Delta \gg V$. In the limit of large defects Δ the eigenstates remain almost unperturbed and the eigenenergies are $E_+ = \hbar\Delta + \frac{V^2}{\hbar\Delta}$ and $E_- = \hbar\Delta - \frac{V^2}{\hbar\Delta}$. Both these energies have a dependence $\frac{C_6}{R^6}$ where $C_6 = C_3/(\hbar\Delta)$. This is the limit of *van der Waals* interaction or induced dipole interaction. The same effect could be derived by second order perturbation theory when the interaction potential V is treated like a small perturbation.

The crossover between these two regimes appears when the coupling strength equals the energy defect $\hbar\Delta \approx V$. A crossover distance between the dipole-dipole and van der Waals regimes can be defined as

$$R_{\text{vdW}} = \left(\frac{C_3}{\hbar\Delta}\right)^{\frac{1}{3}}. \tag{4.6}$$

So for smaller distances than R_{vdW} there are dipolar interactions and for distances larger than R_{vdW} the interactions are of van der Waals type. [7]

4.1.1 C_6 coefficient

The atomic species of interest in the present thesis is Rubidium, in particular the isotope ^{87}Rb. In the experiment reported in this chapter, these atoms are excited to the Rydberg state $70s_{1/2}$ and so, due to the selection rules and the parity of the operator V_{dd}, the main channels to be considered for the van der Waals or dipolar interaction are of the kind

$$s_{1/2} + s_{1/2} \longleftrightarrow p + p \tag{4.7}$$

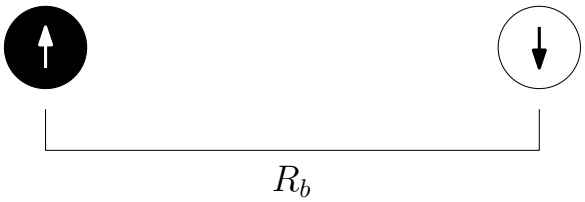

FIGURE 4.1. *Initial conditions for the simulations of internal and external dynamics of a system of two atoms.*

An example could be the interaction $70s_{1/2} + 70s_{1/2} \leftrightarrow 69p_{3/2} + 70p_{3/2}$ which gives the contribution $C_6 = h \cdot 799\,\text{GHz}\,\mu\text{m}^6$ [48].

The full value of the coefficient C_6 for ^{87}Rb atoms in the state $70s$ can be found considering the contribution from all the possible interaction channels like (4.7) and it is [49]

$$C_6 = h \cdot 0.86\ \text{THz}\,\mu\text{m}^6 \tag{4.8}$$

The interaction between two ^{87}Rb atoms in the Rydberg state $70s_{1/2}$ is found to be repulsive.

4.2 Dynamics of a bi-atomic system

Consider a system made of only two atoms of ^{87}Rb placed initially at a distance equal to the facilitation radius $r_{\text{fac}}(\delta)$ (see Chapter 1) for a given detuning δ. For sake of simplicity, lets assume an initial configuration with both the atoms motionless and the rightmost one excited (see Figure 4.1)

When exciting the system off-resonance with a detuning δ, the excitation rate of the left atom is maximum because it is in the facilitation shell of the rightmost one and so it has high probability to be excited. When this happens the atoms are consequently both in the $|\uparrow\rangle$ state and so interact by means of a repulsive van der Waals potential C_6/r^6.

In this situation, just after the second excitation, there are two concurrent effects. The two atoms will find themselves at a distance r_{fac} from each other and so their excitation and de-excitation rates are maximum, successive de-excitations and excitations are very probable

but at the same time they will repel each other with consequent increase of the distance and decreasing of the transition rates, given the form of the rates in the off-resonant case (see Figure 1.3).

The parameter that controls the balance between these two effects is the Rabi frequency Ω. Two different regimes are expected.

- For small Ω the excitation of the second atom will occur later on average but at the same time also the de-excitation process will take longer leaving the atoms the time to repel each other away from their respective facilitation shell.
- For larger Ω the excitation and successive de-excitations will happen faster on average. So it is possible to have multiple flips of the atoms before they repel themselves out of their facilitation shell.

Results of the simulation of the coupled internal and external dynamics for this simple system, are reported in Figure 4.2. The simulations are performed for different Ω and taking $\frac{\delta}{2\pi} = 80\,\text{MHz}$. Each simulation consists of 100 repetitions.

As we can see from Figure 4.2 for values of the Rabi frequency, larger than $2\pi \times 0.6\,\text{MHz}$ the mean number of excited atoms do not change appreciably for $t \geq 5.0\,\mu\text{s}$. We therefore consider the internal dynamics of the system as frozen and only simulate the external dynamics.

4.3 Van der Waals explosion of an atomic cluster

The goal of this experiment is to measure the mechanical effect of the van der Waals interaction among Rydberg atoms. In order to provide data to be comparable with the experiment, the knowledge and understanding of the apparatus is required.

Rubidium-87 atoms are trapped inside a *Magneto-Optical Trap* (MOT) and cooled to a temperature of the order of $\sim 200\,\mu\text{K}$. Then the atoms are excited to the Rydberg state $70s$. After the "expansion time" (τ_e) only atoms in the Rydberg state are ionized and

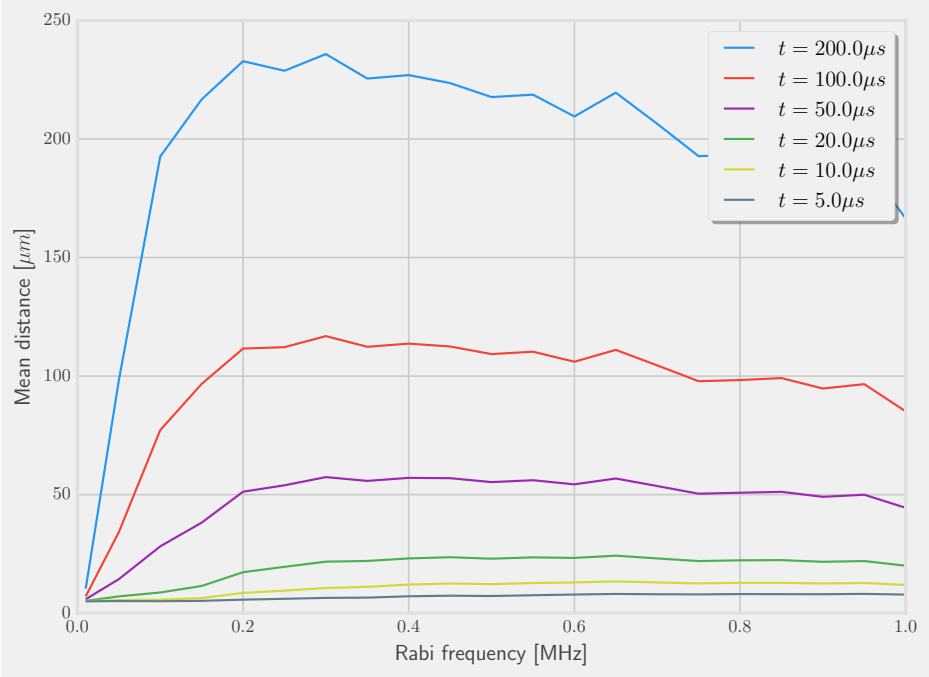

(A) *Plot of the mean distance as a function of the Rabi frequency for different expansion times.*

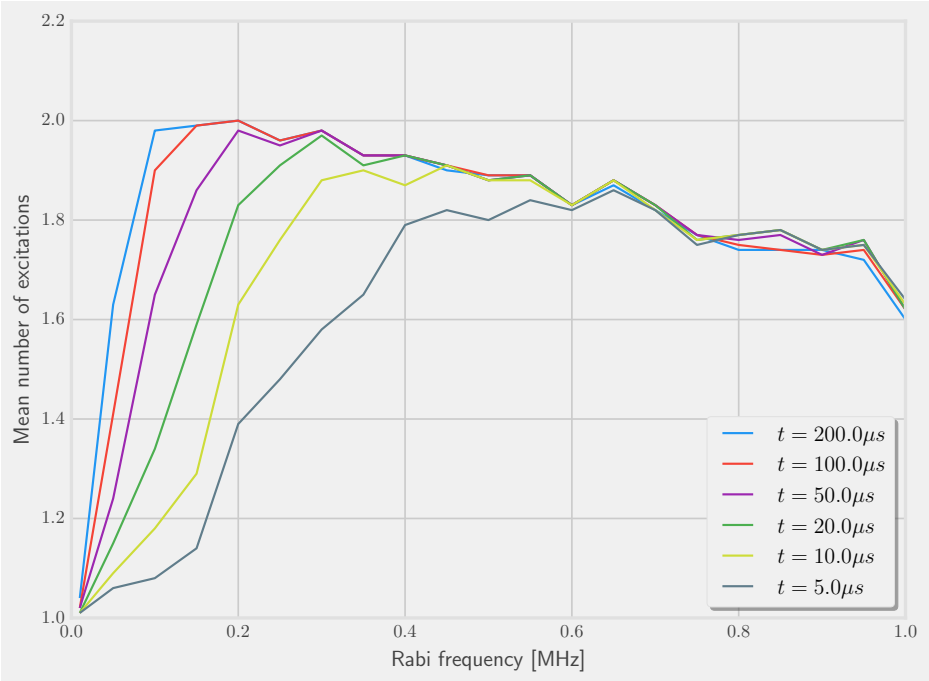

(B) *Plot of the mean number of excitations as a function of the Rabi frequency for different expansion times.*

FIGURE 4.2. *Results of the simulation of the expansion of two Rydberg atoms coupled with the simulation of the internal dynamics.*

then accelerated towards the detector, which is a *Channel Electron Multiplier* (sometimes abbreviated as *CEM* or *Channeltron*).

The detailed description of the apparatus is out of scope for the present thesis. In the following sections will be introduced only the features of the experiment useful to the development and the understanding of the simulations. The discussion is structured so that each time a relevant feature of the experiment is introduced its implications regarding the simulations are discussed.

For further details about the experimental setup we refer to [50, 51].

4.3.1 Trapping and cooling

This experiment uses a magneto-optical trap to produce cold and confined clouds of ^{87}Rb atoms with sizes of the order of a few hundreds micrometers and temperature $\sim 200\,\mu$K.

The cooling effect of the MOT is obtained by using three pairs of counter propagating laser beams. These beams are slightly detuned towards the red from the resonant frequency of the atomic transition of interest. This ensures that atoms which move towards the laser source, because the Doppler shift are more likely to absorb the incoming photons. The momentum is conserved in the absorption process so the atoms which absorb the light undergo a changing momentum of $\hbar\omega_{\text{laser}}$ opposite to their direction of motion. Averaged on many absorption processes, this results in an effective friction force that ultimately causes the cooling of the cloud.

The trapping instead is obtained by means of a spatially varying magnetic quadrupole field causing a Zeeman shift of the atomic levels dependent on the position. The magnetic field is engineered in a way that atoms moving away from the center of the trap have levels shifted so they are resonant with the incoming photons. So atoms that are fleeing away will pushed back towards the center of the trap. [52]

The structure of the levels involved in the trapping and cooling processes is shown in Figure 4.3. The trapping and cooling loop is driven by the TRAP laser which is detuned by

Δ from the transition $\left|5S_{1/2},\, F=2\right\rangle \rightarrow \left|5P_{3/2},\, F'=3\right\rangle$. It is possible, in this process, that atoms will be excited off-resonantly to the $\left|5P_{3/2},\, F'=2\right\rangle$ level. From this level there are two possible decay channels, one towards the state $\left|5S_{1/2},\, F=2\right\rangle$ and another towards $\left|5S_{1/2},\, F=1\right\rangle$. Atoms that end up in the $F=1$ state will stop cycling between the ground state and the excited state and so the cooling and the trapping for these atoms stops. Therefore, another laser source termed REPUMP and tuned to the transition $\left|5S_{1/2},\, F=1\right\rangle \rightarrow \left|5P_{3/2},\, F'=2\right\rangle$, is needed to recycle these atoms back in the loop so that the cooling and the trapping can continue.

4.3.2 Excitation to Rydberg states

Atoms of ^{87}Rb are excited to the Rydberg state $70s_{1/2}$ in a two-photon process. To obtain the excitation, two different laser sources are used, one at 420 nm (blue) detuned by $\delta = 660$ MHz from the transition $\left|5s_{1/2}\right\rangle \rightarrow \left|6p_{3/2}\right\rangle$ in order to avoid the population of the level $\left|6p_{3/2}\right\rangle$, while the second is at 1013 nm (infrared) and tuned to reach the Rydberg state. [53, 54]

The generalized Rabi frequency for the two-photon excitation process is given by

$$\Omega = \sqrt{\frac{\Omega_{\text{blue}}^2 \Omega_{\text{infrared}}^2}{4\delta^2} + \Delta^2} \tag{4.9}$$

where Δ is the detuning from the transition to the Rydberg state, Ω_{blue} is the Rabi frequency of the excitation (driven by the blue laser) and Ω_{infrared} is the Rabi frequency of the second step of the excitation (driven by laser @1013nm)

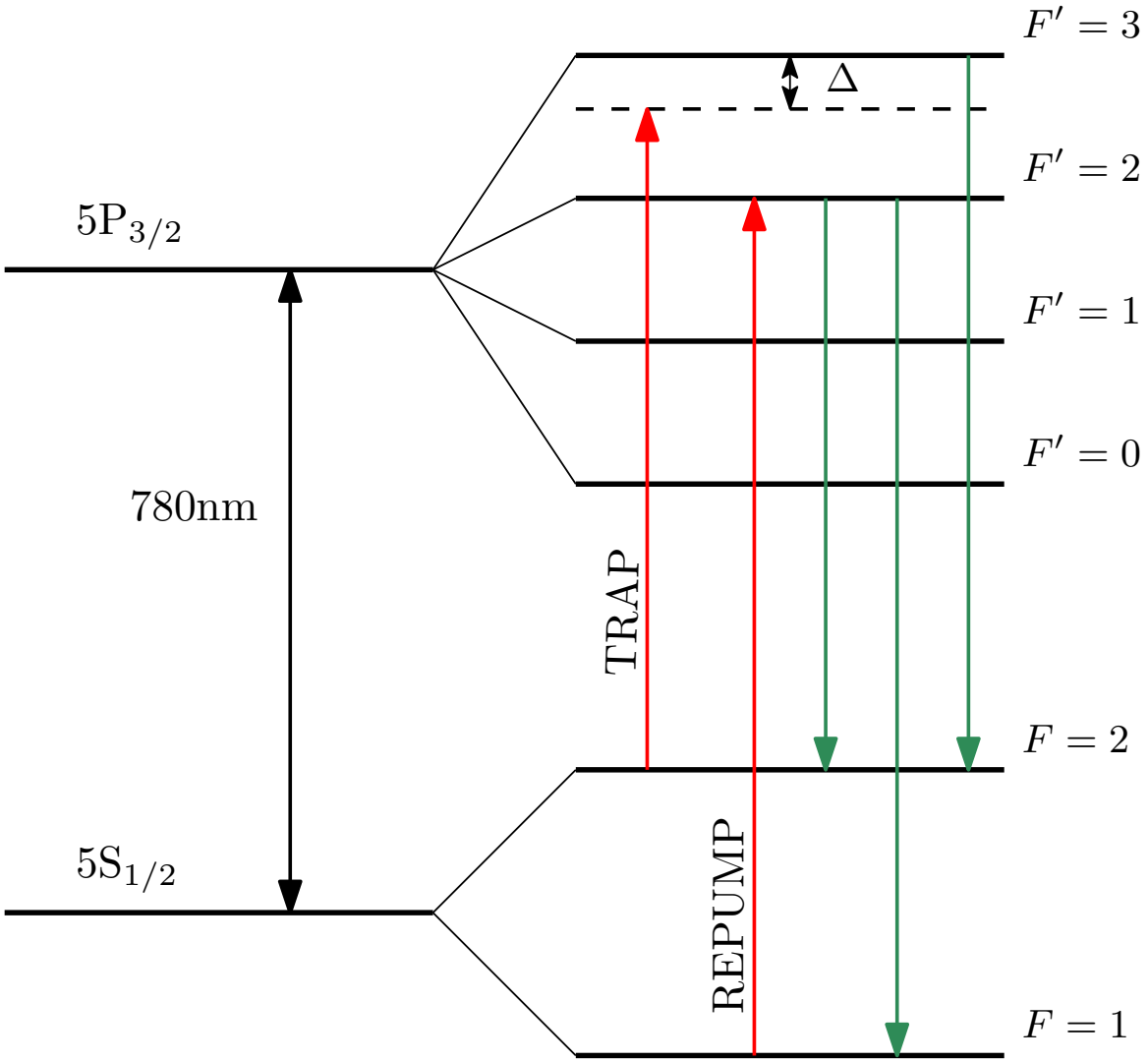

FIGURE 4.3. *Levels involved in the Magneto-Optical Trap. Green arrows indicate the main decay channels while red arrows indicate the* TRAP *and* REPUMP *absorption processes.*

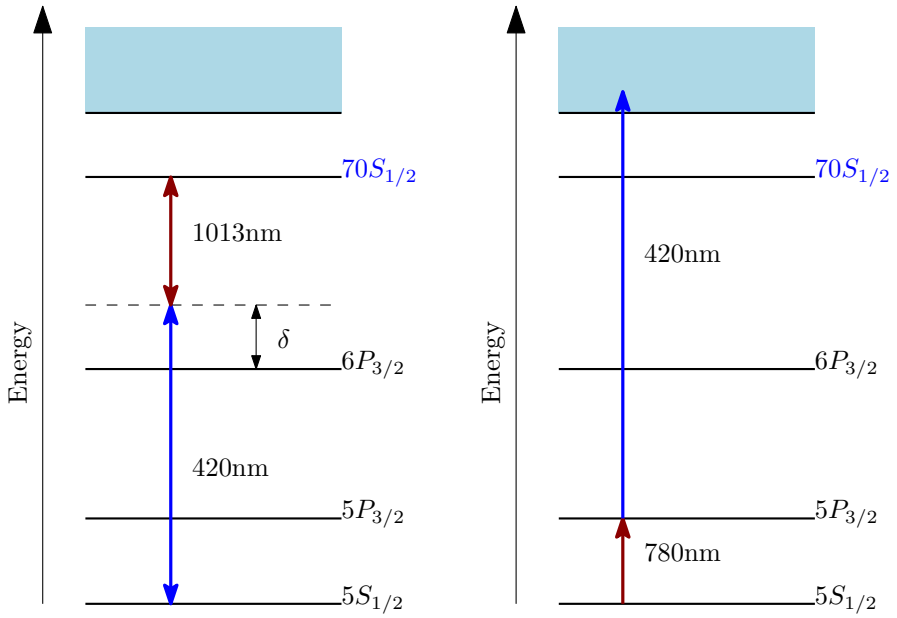

(A) *The excitation to the Rydberg state* $70s_{1/2}$ *is a two-photon process.* $\delta \approx 660MHz$.

(B) *When the fields of the* MOT *are turned on the blue laser @480nm ionizes the Rubidium atoms.*

FIGURE 4.4. *Excitation processes of* ^{87}Rb.

The geometry of the beams into the quartz cell is shown in Figure 4.5. In this configuration the blue laser is focused to a waist of $6\,\mu$m, which is comparable to the facilitation radius r_{fac} while the infrared laser is focused to a waist of about $110\,\mu$m and tilted by 45 degrees with respect to the direction of the blue laser. In this configuration the interaction volume, that is the volume in which Rydberg excitations are created, is almost one-dimensional and so the resulting system is a chain of Rydberg atoms.

As seen in Chapter 3 off-resonant excitation processes ($\Delta \neq 0$) can lead to the formation of cluster of Rydberg atoms where the distances between the atoms are equal to the facilitation radius r_{fac}. In the case on resonance, instead, the distances between the atoms will be greater than the blockade radius R_b. We expect that the magnitude of the effect to be observed (the expansion of the system of Rydberg atoms) will depend on the total initial potential of the system. Given the form C_6/r^6 of the van der Waals interaction, this potential will be greater for shorter initial distances of the atoms. For these reasons the experiment is performed with three different regimes of excitation:

- on resonance, where $\Delta = 0$ and $R_b = 10.946\,\mu$m;
- off resonance with $\frac{\Delta}{2\pi} = 55\,$MHz, where the facilitation radius is $r_{\text{fac}} = 5\,\mu$m;
- off resonance with $\frac{\Delta}{2\pi} = 80\,$MHz, where the facilitation radius is $r_{\text{fac}} = 4.698\,\mu$m.

In all of these processes the excitation is carried out until an average of 12 excitations are created.

The off-resonance excitations are performed by inserting a *seed* in the system at $t = 0$, namely a resonant excitation, and then starting to excite the system off resonance. The insertion of the seed facilitates the off-resonant dynamics of its neighbor with the possibility to start an avalanche excitation process and so the creation of clusters of Rydberg atoms.

4.3.3 Creation of the cluster and initial conditions for the equation of motion

The initial system, which will be used as the starting point in the integration of the equations of motion, can be modelled using the knowledge of both the excitation process and the geometry of the apparatus. In the simplest scheme possible the atoms will form a perfect one-dimensional chain parallel to the direction of the blue laser, with the distance between the atoms of the chain depending on the detuning.

In the off-resonant case the resulting cluster of Rydberg atoms will be characterized by distance between the atoms equal to the facilitation facilitation radius r_{fac}. Also if the interaction volume is almost one-dimensional, the resulting system will be a chain with spacing r_{fac}. Variations from the simple chain model include displacements of the atoms in the direction perpendicular to the blue beam. Since the probability of creating an excitation at a given point in space is proportional to Ω^2, and hence to the intensity of the excitation laser in that point, the perpendicular displacements are sampled, in the simulation from a gaussian distribution having as standard deviation $\frac{waist_{\text{blue}}}{2}$ and centered onto the direction of the blue beam. This "chain", in the simulation, is created in such a way that the distances between an atom and its neighbors are exactly r_{fac}.

In the resonant regime the excitation dynamics is subject to the effect of the blockade where two excitations at distances less than the blockade radius strongly suppressed. The initial position of the atoms in this case are then sampled from a multivariate normal distribution

$$f(x,y,z) = \frac{1}{2\pi\sigma_x\sigma_y\sigma_z}\exp\left[-\frac{1}{2}\left(\frac{x^2}{\sigma_x^2}+\frac{y^2}{\sigma_y^2}+\frac{z^2}{\sigma_z^2}\right)\right] \tag{4.10}$$

with the added constraint that the distance between the atoms has to be at least the blockade radius R_b. The standard deviations of the distribution in the plane (y,z) are given by the waist of the blue beam ($\sigma_y = \sigma_z = \frac{\text{waist}_{\text{blue}}}{2}$) while in the direction parallel to the blue beam the standard deviation is given by the size of the mot $\sigma_x = \sigma_x^{\text{mot}}$.

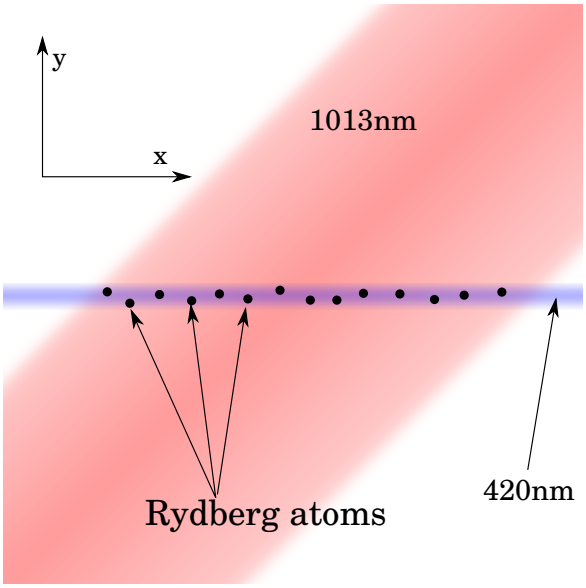

FIGURE 4.5. *Schematic of the 1D configurations of the beams. The angle between the beam @420nm and the other @1013nm is* 45°

Velocities The temperature of the MOT can be estimated to be $\approx 200\mu$K and we assume that the initial velocities of the atoms in the chain are given by the Maxwell-Boltzmann distribution

$$f_{\mathbf{v}}(v_x, v_y, v_z) = \left(\frac{m}{2\pi kT}\right)^{3/2} \exp\left[-\frac{m(v_x^2 + v_y^2 + v_z^2)}{2kT}\right] \tag{4.11}$$

which is simply a multivariate normal distribution with $\sigma_x = \sigma_y = \sigma_z = \sqrt{\frac{kT}{m}} \approx 0.138\frac{\text{m}}{\text{s}}$ where k is the Boltzmann constant and m is the mass of the atoms.

The initial positions and velocities are the starting point for the integration of the equation of motion of the system. Since they are sampled randomly, each shot of the simulated experiment will start with different initial conditions.

4.3.4 The detection apparatus

A simple schematic of the detection apparatus is shown in Figure 4.6. After the creation of a cluster of Rydberg atoms, a variable time τ_e is waited to let the system expand. Then the

atoms are ionized and accelerated towards the detector by applying a tension of 3.5kV to the front plates and -1kV to the lateral ones. The particles are then directed towards the detector by a grid with a voltage of $(1150 \pm 10)V$.

The channeltron detects incoming charged particles producing a current signal each time a particle arrives on its sensitive surface. An example signal is shown in Figure 4.7 where each peak corresponds to the detection of a single ion.

The detection efficiency of the entire apparatus is estimated to be about $\eta \approx 0.4$ which means that only the 40% of the incoming ions are detected.

Coulomb repulsion After the ionization and during their flight towards the channeltron the ions, which have charge $+e$, interact by means of a repulsive Coulomb potential which is $\propto 1/r$. So the Coulomb repulsion between the ions is taken into account in the simulations for the entire time between the ionization of the Rydberg atoms and the arrival of the cluster to the channeltron. This time is measured to be $\tau_{\text{flight}} \approx 10\mu$s. So after solving the equation of motion in the presence of the van der Waals interaction for a time τ_e we integrate the new equations of motion which include only the Coulomb repulsion between the ions for a time τ_{flight} using as initial condition, the positions and velocities just before the ionization process.

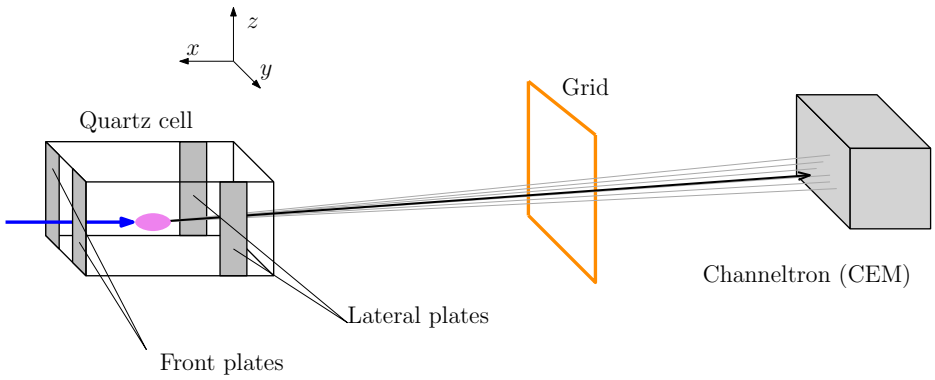

FIGURE 4.6. *Schematic of the experimental apparatus. The* MOT *is formed inside the quartz cell on which are placed two pairs of electrical plates at high voltage which ionize the Rydberg atoms and accelerate the ions towards the* CEM*. The* GRID *is placed next to the cell and prior the* CEM*. In the figure the components are not in scale with each other.*

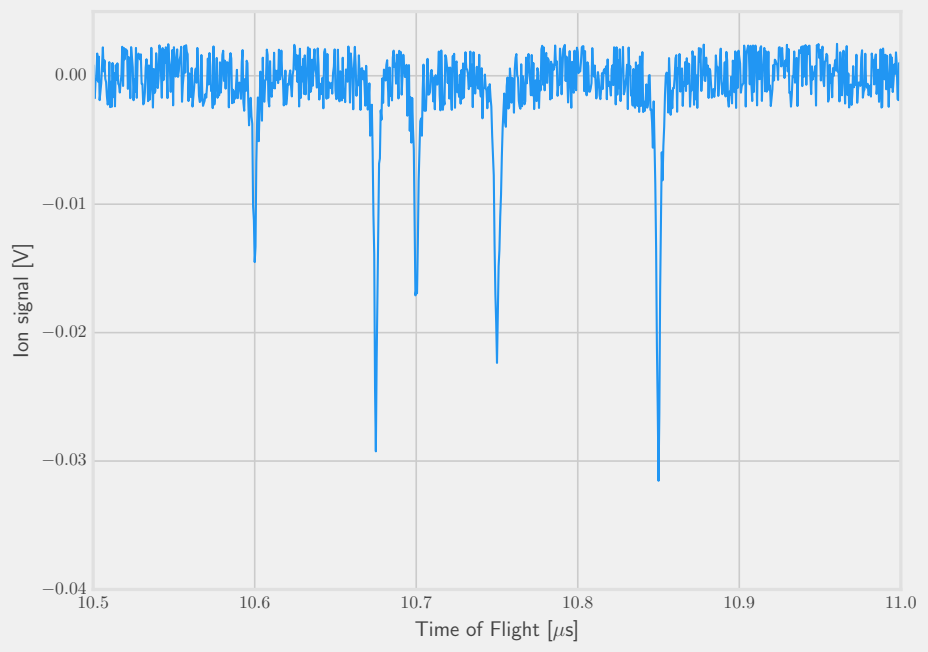

FIGURE 4.7. *Example of the signal generated by the* CEM

4.3.5 Distribution of arrival times

Information about the position of the atoms inside the quartz cell are available only through the analysis of the arrival times of the ions at the detector.

In both the simulations and the experiment the distribution of the arrival times, like the ones in Figure 4.8a, are obtained through multiple repetitions of the expansion. Each repetition is called a *shot* while the term *experiment* or *simulations* refer to the whole ensemble of shots.

The number of shots executed in each experiment is 400 while it is 1000 in the simulations.

The distributions of the arrival times, like the one in Figure 4.8a or in Figure 4.8c are fitted with gaussian functions and the standard deviations of the fit functions is taken as a measure of the width of the atomic cluster.

The comparison of the distributions obtained in the experiment with the ones in the simulations is done by converting the positions of the atoms obtained from the simulations in arrival times through a relation

$$t_{\text{arrival}} \equiv t_{\text{arrival}}(x, y, z) \tag{4.12}$$

Then the distribution of arrival times obtained are fitted with gaussian functions and compared tho the experimental ones.

In order to have a valid conversion from positions to the arrival times, like the one in equation (4.12), a calibration of the detection apparatus is needed. The calibration is performed moving a MOT inside the quartz cell and comparing the coordinates of its centers, obtained with the use of a CCD camera, with the center of the distribution of the arrival times of the ions created by direct ionization of (on average) a single atom in the MOT (using the process illustrated in Figure 4.4b) The detailed description of the techniques used to perform the calibration of the apparatus are argument of the thesis by *M. Archimi* [47, pp. 25-34].

From the data plotted in figure 4.9 it is clear that the calibration of the arrival times is

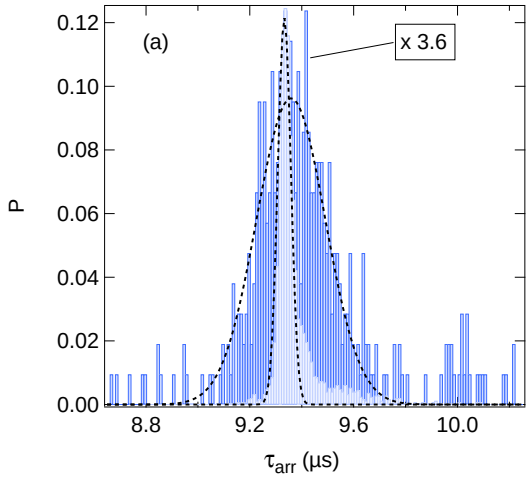

(A) *Two different experimental distributions of the arrival times for two different values of the expansion time $\tau_e = 130\mu s$ (light blue bars) and $\tau_e = 1000\mu s$ (dark blue bars) with the corresponding gaussian fits (black dashed lines).*

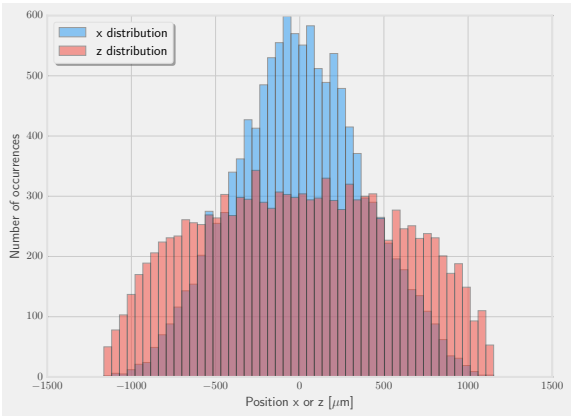

(B) *Distributions of the position of the atoms along the x (blue bars) and z (red bars) directions for an expansion time $\tau_e = 1000\mu s$*

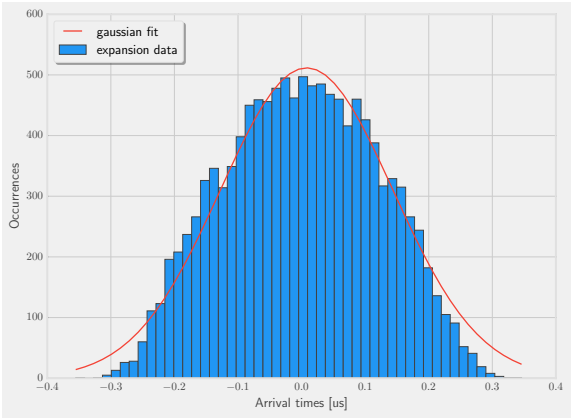

(C) *Distribution of the arrival times obtained from the simulations and applying the calibration and fitted with a gaussian function (dark red line).*

FIGURE 4.8. *Comparison of the distribution of arrival times in the experiment and the distribution of the positions in the simulations.*

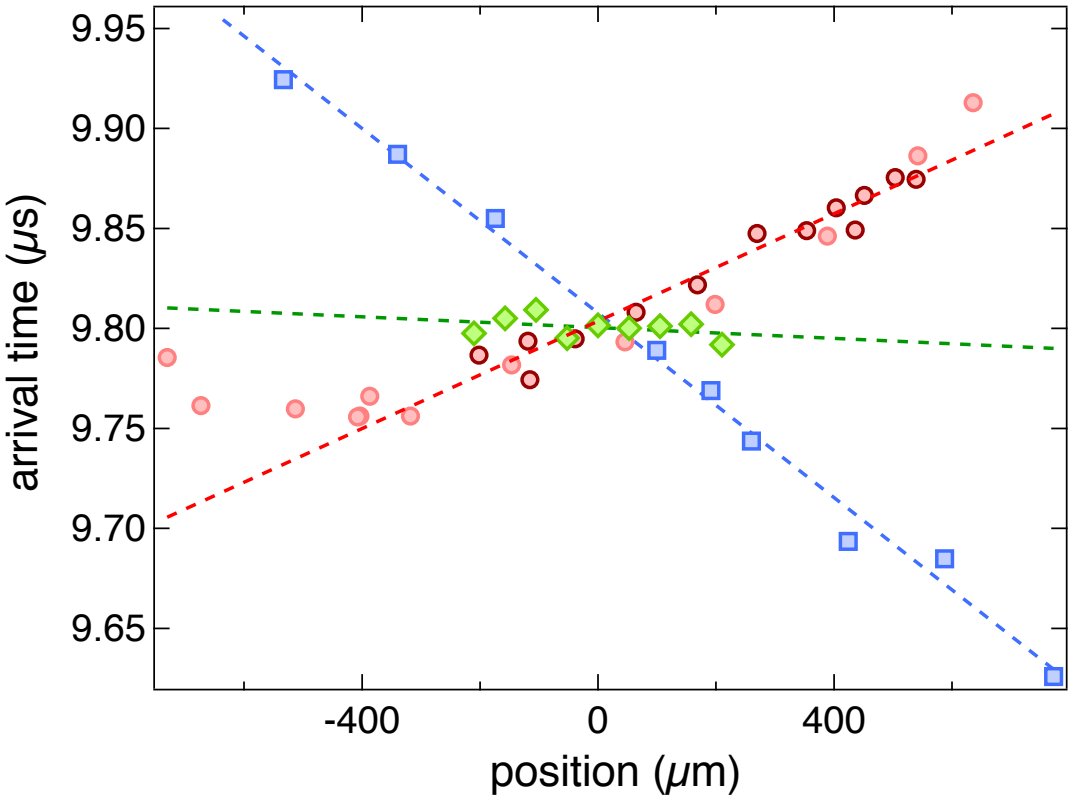

FIGURE 4.9. *Calibration of the arrival times along the directions x (blue), y (green) and z (red). The dark red points represent another calibration along the z axis for a different value of x in order to check the linearity of the whole calibration.*

Coefficient	Value
α	$(-2.31 \pm 0.08)10^{-4}\frac{\mathrm{m}}{\mathrm{s}}$
β	$(-0.134 \pm 0.126)10^{-4}\frac{\mathrm{m}}{\mathrm{s}}$
γ	$(1.34 \pm 0.07)10^{-4}\frac{\mathrm{m}}{\mathrm{s}}$

TABLE 4.1. *Coefficients of the calibration*

linear in the positions x, y, z and takes the form

$$t_{\text{arrival}}(x, y, z) = \alpha x + \beta y + \gamma z \tag{4.13}$$

and the values of the coefficients are reported in table 4.1. Applying the calibration 4.13 to data obtained from the simulations yields the results showed in Figure 4.8c which can be easily compared to the data obtained from the experiment.

From the relation (4.13) and the values of the coefficients given in Table 4.1 it is easy to see that the detection process projects ions created in an isochronous plane onto a particular arrival time at the channeltron. These isochronous planes, which contain the y axis, enclose an angle of $(59.9 \pm 1.5)^\circ$ with the $x - y$ plane.

While the equation (4.13) offers a convenient way to convert the spatial information for a single particle in its arrival times the "inverse" is not possible. The only spatial information available from the relative arrival time Δt of two particle is their distance Δs perpendicular to the isochronous planes

$$\Delta s = \frac{\Delta t}{\sqrt{\alpha^2 + \beta^2}} \quad \text{with} \quad \sqrt{\alpha^2 + \beta^2} = 2.67 \pm 0.08 \times 10^{-4}\frac{\mathrm{m}}{\mathrm{s}} \tag{4.14}$$

4.3.6 Results

We performed three different experiments in order to obtain the time dependence of the cluster size in tree different regimes

- on resonance,

- off resonance with $\Delta = 2\pi \times 80\,\text{MHz}$,
- off resonance with $\Delta = 2\pi \times 55\,\text{MHz}$.

The results are presented in Figure 4.11. The expansion of the cluster is clearly visible for $\frac{\Delta}{2\pi} = 80\,\text{MHz}$ (red circles) and $\frac{\Delta}{2\pi} = 55\,\text{MHz}$ (blue squares) while it is negligible in the case of resonant excitations, $\Delta = 0$. This is expected because in the resonant case, because of the blockade effect, the distances between the excitations are larger than in the two off-resonant cases and so the atoms will feel a negligible van der Waals repulsion resulting in an expansion purely due to the thermal motion of the atoms. The larger the detuning, the shorter will be the facilitation radius and so the initial distance between the atoms. So for larger detunings we expect the initial total potential energy of the system to be larger and so the effect of the expansion. This can be easily seen from the comparison of the expansions at 55 MHz and 80 MHz where the expansion of the case at 80 MHz is larger than the case at 55 MHz

The plots in Figure 4.10 represents the outcome of a single shot of the initial simulation. In 4.10a the trajectories of the particles during the first tens of micro seconds are plotted. In 4.10b the time evolution of the velocities is plotted. From the Figure 4.10a can be observed that the velocity of the expansion along the y-axis is greater than along the x-axis.

As can be seen from Figure 4.11 below the 200μs of expansion time there is a slight disagreement between the simulation and the experimental data. It appears that the simulations overestimate the effect of the Coulomb repulsion during the flight of the ions towards the channeltron which is more evident for shorter expansion times. Even if no simple explanation of this effect has been found so far, maybe this is due to our incomplete knowledge of the exacts trajectories of the ions.

The simulations, that are presented in Figure 4.11 as dashed lines of the same color as the experimental data they refer to, are in good agreement with the experiment for longer times. This constitutes a direct observation of the mechanical effect of the van der Waals interaction upon clusters of Rydberg atoms.

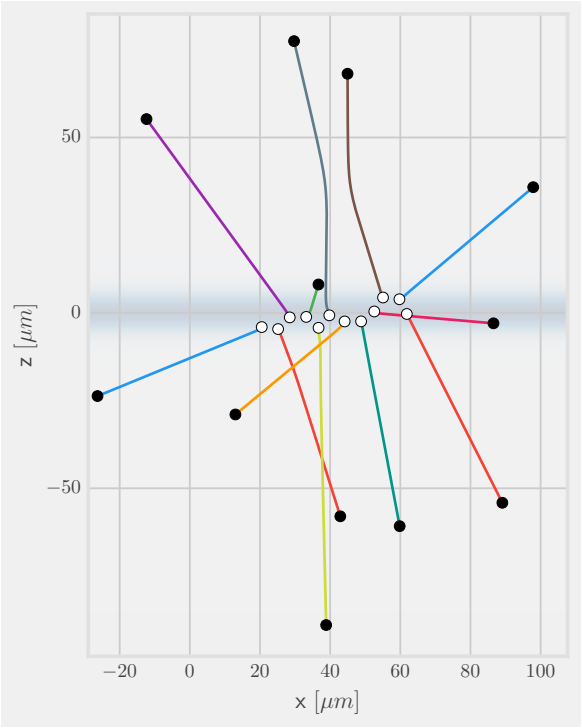

(A) *Trajectories. The white circles represent the initial positions of the atoms, while the black circles represents the position at the end of the expansion. The blue blurred line along the x axis is representative of the shape and the dimensions of the blue beam used in the excitation process.*

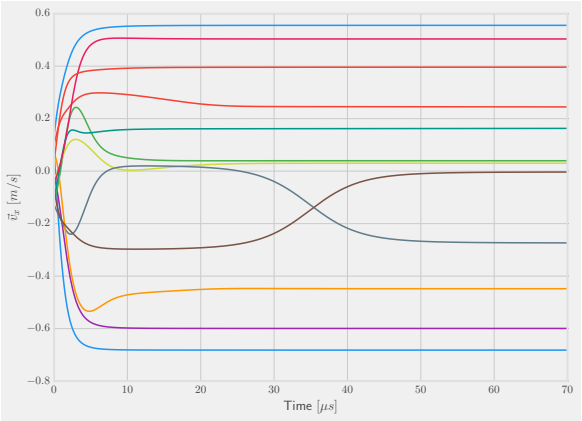

(B) *Velocities along the x axis*

FIGURE 4.10. *Trajectories and velocities are plotted for the firsts 70μs for the expansion at 80MHz*

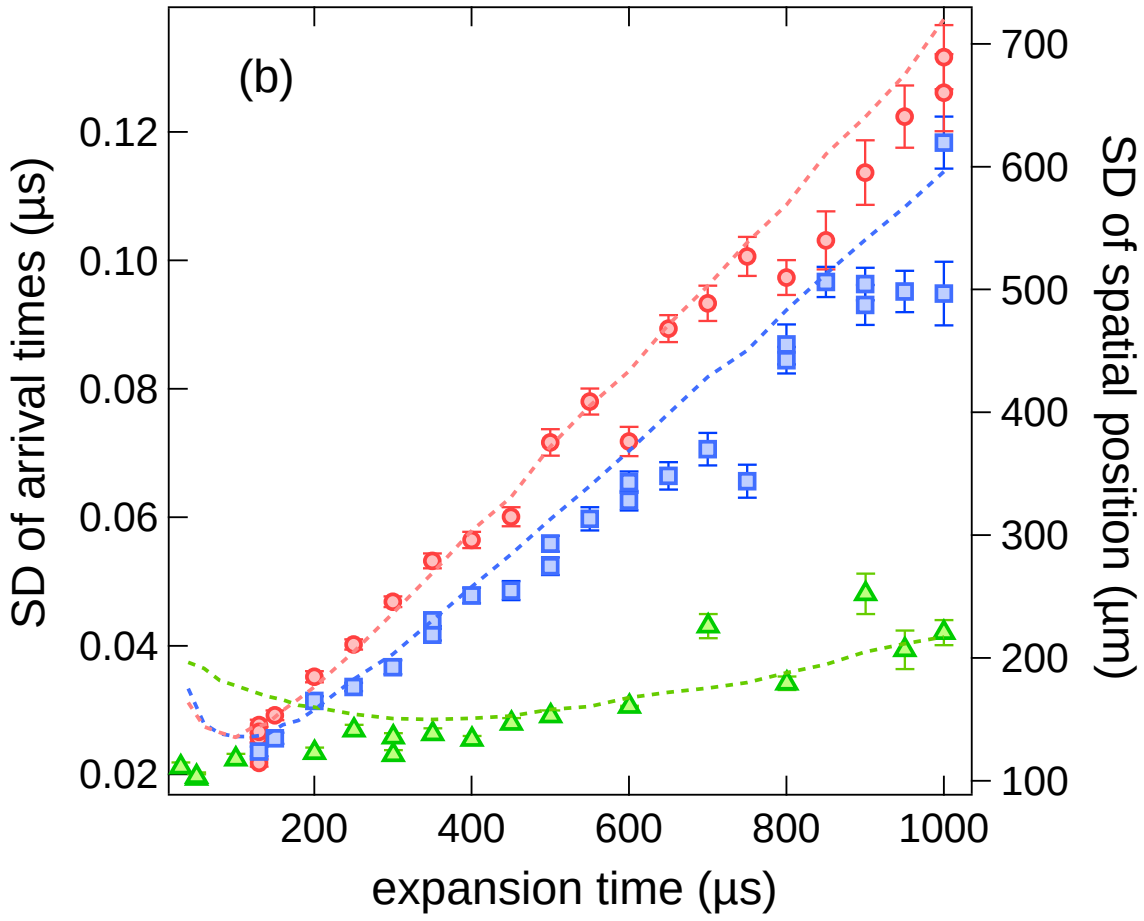

FIGURE 4.11. *Standard deviations of the ion cloud distribution are plotted as a function of the expansion time for different detunings δ: 0 (green triangles), 55 (blue squares) and 80MHz (red circles). On the left hand side axis there are the standard deviations of the arrival times while on the right hand side axis there are the standard deviations of the spatial positions obtained using the relation 4.14. The dashed lines represent the results obtained from the numerical simulations of the expansion.*

Chapter 5

Conclusions

In this thesis we performed a numerical study of the dynamics out of equlibrium of a many-body system composed of strongly interacting Rydberg atoms. This study has been done by decoupling the dynamics of the internal and external degrees of freedom of the system.

To understand the non trivial behaivour of these system approaching the equilibrium we used a simple model of an Ising spin system with long-range interactions among the spins. The equations of motion for the internal dynamics have been solved by means of Kinetic Monte Carlo methods. The effects of the long range interaction among the spins are studied upon a one-dimensional regular lattice. In the case of resonant excitation process we observed the dramatic slowing down of the dynamics due to the *blockade effect*, where the presence of an excited atom suppress the excitation dynamics of its neighbors. In the off-resonant case we observed facilitated dynamics of atoms and discussed how this effect can lead to the formation of clusters of Rydberg atoms and how can be used to control the state of the system and its dynamics out of equilbrium.

Rydberg atoms are known to interact by means of Van der Waals potential of the form C_6/r^6 [6, 7]. In this thesis we presented an experiment to directly observe the mechanical effects of the Van der Waals forces and developed a method to perform numerical simulations to be directly compared with experimental data. The experiment has been performed in the

laboratory [47] and both the experimental data and the numerical simulations have been published on the preprint server and submitted to Physical Review Letters [32].

The main effort of the present thesis has been made in the development and in the implementation of efficient algorithms to simulate the out of equilibrium dynamics of these systems. The actual code used has been entirely written by the author using C, C++ and Julia[1] [55, 56] languages and consists of more than $3K$ lines of code. The software and libraries developed can handle different kind of systems, lattices, gasses etc. Further improvements of this software are planned and include the implementaton of efficient algorithms for k-nearest neighbor search [57] using GPU or the improvement of the parallelization of these algorithms through the extension of the currently used method [58] to the case of long range interactions.

5.1 Outlook

The study of the internal dynamics of the many-body system introduced in the present thesis has been done in the case of incoherent dynamics, namely under the assumption that the density-matrix of the system is diagonal describing then a classical state. Further studies can explore the coherent dynamics of these systems trying to synthesize from the exact solutions of the dynamics of few-body systems the governing principles for the macroscopic behaviour of a many-body system.

In this thesis we have studied the response of a system of Rydberg atom subject to sudden changes of the excitation parameters (ie. the detuning). A generalization of this work can be the study of the out of equilibrium dynamics of the system under continuous changes of the excitation parameters such as sweeps in the detuning.

These studies can be used to develop sophisticated and precise experimental techniques to control the creation of aggregates of Rydberg atoms with given properties.

[1] a new modern language for technical computing developed at MIT http://julialang.org

Bibliography

[1] P. Coleman. *Introduction to Many-Body Physics*. Cambridge University Press, 2015, p. 766 (cit. on p. vii).

[2] P. W. Anderson. "More Is Different". In: *Science (80-.).* 177.4047 (Aug. 1972), pp. 393–396. DOI: 10.1126/science.177.4047.393 (cit. on p. vii).

[3] J. Eisert, M. Friesdorf, and C. Gogolin. "Quantum many-body systems out of equilibrium". In: *Nat. Phys.* 11.2 (Feb. 2015), pp. 124–130. DOI: 10.1038/nphys3215 (cit. on p. vii).

[4] I. Mourachko, D. Comparat, F. de Tomasi, A. Fioretti, P. Nosbaum, V. M. Akulin, and P. Pillet. "Many-Body Effects in a Frozen Rydberg Gas". In: *Phys. Rev. Lett.* 80.2 (Jan. 1998), pp. 253–256. DOI: 10.1103/PhysRevLett.80.253 (cit. on p. vii).

[5] S. G. Brush. "History of the Lenz-Ising model". In: *Rev. Mod. Phys.* 39.4 (1967), pp. 883–893. DOI: 10.1103/RevModPhys.39.883 (cit. on p. viii).

[6] T. F. Gallagher. *Rydberg Atoms*. Cambridge University Press, 2005 (cit. on pp. viii, 71).

[7] D. Comparat and P. Pillet. "Dipole blockade in a cold Rydberg atomic sample". In: (2010). DOI: 10.1364/JOSAB.27.00A208. arXiv: 1006.0742 (cit. on pp. viii, 6, 49, 71).

[8] C. Ates and I. Lesanovsky. "Entropic enhancement of spatial correlations in a laser-driven Rydberg gas". In: *Phys. Rev. A* 86.1 (July 2012), p. 013408. DOI: 10.1103/PhysRevA.86.013408 (cit. on p. 2).

[9] A. A. Ovchinnikov, D. V. Dmitriev, V. Y. Krivnov, and V. O. Cheranovskii. "Antiferromagnetic Ising chain in a mixed transverse and longitudinal magnetic field". In: *Phys. Rev. B* 68.21 (Dec. 2003), p. 214406. DOI: 10.1103/PhysRevB.68.214406. arXiv: 0306468 [cond-mat] (cit. on p. 2).

[10] I. Lesanovsky and J. P. Garrahan. "Kinetic constraints, hierarchical relaxation, and onset of glassiness in strongly interacting and dissipative rydberg gases". In: *Phys. Rev. Lett.* 111.21 (2013), pp. 1–5. DOI: 10.1103/PhysRevLett.111.215305. arXiv: arXiv:1307.8078v1 (cit. on pp. 2, 3, 14, 31, 33, 42, 45).

[11] H.-P. Breuer and F. Petruccione. *The Theory of Open Quantum Systems*. Oxford University Press, Jan. 2007. DOI: 10.1093/acprof:oso/9780199213900.001.0001 (cit. on p. 2).

[12] M. A. Schlosshauer. *Decoherence: And The Quantum-To-Classical Transition*. Springer, 2007, p. 417 (cit. on p. 2).

[13] G. Lindblad. "On the generators of quantum dynamical semigroups". In: *Commun. Math. Phys.* 48.2 (1976), pp. 119–130. DOI: 10.1007/BF01608499 (cit. on p. 2).

[14] R. Löw, H. Weimer, J. Nipper, J. B. Balewski, B. Butscher, H. P. Büchler, and T. Pfau. "An experimental and theoretical guide to strongly interacting Rydberg gases". In: *J. Phys. B At. Mol. Opt. Phys.* 45.11 (2012), p. 113001. DOI: 10.1088/0953-4075/45/11/113001. arXiv: arXiv:1202.2871v1 (cit. on p. 4).

[15] F. Robicheaux and J. V. Hernández. "Many-body wave function in a dipole blockade configuration". In: *Phys. Rev. A - At. Mol. Opt. Phys.* 72.6 (2005), pp. 4–7. DOI: 10.1103/PhysRevA.72.063403 (cit. on p. 4).

[16] A. Bortz, M. Kalos, and J. Lebowitz. "A new algorithm for Monte Carlo simulation of Ising spin systems". In: *J. Comput. Phys.* 17.1 (Jan. 1975), pp. 10–18. DOI: 10.1016/0021-9991(75)90060-1 (cit. on p. 14).

[17] N. Metropolis, A. W. Rosenbluth, M. N. Rosenbluth, A. H. Teller, and E. Teller. "Equation of State Calculations by Fast Computing Machines". In: *J. Chem. Phys.* 21.6 (1953), pp. 1087–1092. DOI: doi:10.1063/1.1699114. arXiv: 5744249209 (cit. on p. 14).

[18] K. Reuter. "First-Principles Kinetic Monte Carlo Simulations for Heterogeneous Catalysis: Concepts, Status, and Frontiers". In: *Model. Simul. Heterog. Catal. React.* (2011), pp. 71–111. DOI: 10.1002/9783527639878.ch3 (cit. on p. 14).

[19] A. Jansen. *An Introduction to Kinetic Monte Carlo Simulations of Surface Reactions*. Vol. 856. Lecture Notes in Physics. Berlin, Heidelberg: Springer Berlin Heidelberg, 2012. DOI: 10.1007/978-3-642-29488-4. arXiv: 0303028 [cond-mat] (cit. on pp. 14, 18, 19).

[20] A. Chernov and J. Lewis. "Computer model of crystallization of binary systems; Kinetic phase transitions". In: *J. Phys. Chem. Solids* 28.11 (Nov. 1967), pp. 2185–2198. DOI: 10.1016/0022-3697(67)90243-0 (cit. on p. 14).

[21] M. Kotrla. "Numerical simulations in the theory of crystal growth". In: *Comput. Phys. Commun.* 97.1-2 (Aug. 1996), pp. 82–100. DOI: 10.1016/0010-4655(96)00023-9 (cit. on p. 14).

[22] T. Garnier and M. Nastar. "Coarse-grained kinetic Monte Carlo simulation of diffusion in alloys". In: *Phys. Rev. B* 88.13 (Oct. 2013), p. 134207. DOI: 10.1103/PhysRevB.88.134207 (cit. on p. 14).

[23] A. Chotia, M. Viteau, T. Vogt, D. Comparat, and P. Pillet. "Kinetic Monte Carlo modeling of dipole blockade in Rydberg excitation experiment". In: *New J. Phys.* 10 (2008). DOI: 10.1088/1367-2630/10/4/045031. arXiv: 0803.4481 (cit. on pp. 14, 18).

[24] D. T. Gillespie. "Exact stochastic simulation of coupled chemical reactions". In: *J. Phys. Chem.* 81.25 (Dec. 1977), pp. 2340–2361. DOI: 10.1021/j100540a008 (cit. on p. 18).

[25] J. M. Sanz-Serna. "Symplectic integrators for Hamiltonian problems: an overview". In: *Acta Numer.* 1 (Jan. 1992), p. 243. DOI: 10.1017/S0962492900002282 (cit. on p. 22).

[26] E. Hairer, S. P. Nørsett, and G. Wanner. *Solving Ordinary Differential Equations I.* Vol. 8. Springer Series in Computational Mathematics. Berlin, Heidelberg: Springer Berlin Heidelberg, 1993. DOI: 10.1007/978-3-540-78862-1 (cit. on pp. 22, 25).

[27] H. Yoshida. "Recent progress in the theory and application of symplectic integrators". In: *Celest. Mech. Dyn. Astron.* 56.1-2 (1993), pp. 27–43. DOI: 10.1007/BF00699717 (cit. on p. 25).

[28] E. Forest and R. D. Ruth. "Fourth-order symplectic integration". In: *Phys. D Nonlinear Phenom.* 43.1 (1990), pp. 105–117. DOI: 10.1016/0167-2789(90)90019-L (cit. on p. 25).

[29] D. Okunbor and R. D. Skeel. "Explicit Canonical Methods for Hamiltonian Systems". In: *Math. Comput.* 59.200 (1992), pp. 439–455 (cit. on p. 25).

[30] M. P. Calvo and J. M. Sanz-Serna. "High-Order Symplectic Runge–Kutta–Nyström Methods". In: *SIAM J. Sci. Comput.* 14.5 (Sept. 1993), pp. 1237–1252. DOI: 10.1137/0914073 (cit. on p. 26).

[31] W. Oevel and Y. B. Suris. *1-parameter families of maximal order Runge-Kutta-Nyström methods.* 1996 (cit. on p. 26).

[32] R. Faoro, C. Simonelli, M. Archimi, G. Masella, M. M. Valado, E. Arimondo, R. Mannella, D. Ciampini, and O. Morsch. "Van der Waals explosion of cold Rydberg clusters". In: (2015), pp. 1–5. arXiv: 1506.08463v1 (cit. on pp. 32, 72).

[33] N. Thaicharoen, a. Schwarzkopf, and G. Raithel. "Measurement of van-der-Waals interaction by atom trajectory imaging". In: 48109.c (2015), pp. 1–6. arXiv: 1506.02705v1 (cit. on p. 32).

[34] I. Lesanovsky. "Many-Body Spin Interactions and the Ground State of a Dense Rydberg Lattice Gas". In: *Phys. Rev. Lett.* 106.2 (Jan. 2011), p. 025301. DOI: 10.1103/PhysRevLett.106.025301 (cit. on p. 33).

[35] L. Mandel. "Squeezed States and Sub-Poissonian Photon Statistics". In: *Phys. Rev. Lett.* 49.2 (July 1982), pp. 136–138. DOI: 10.1103/PhysRevLett.49.136 (cit. on p. 35).

[36] C. Ates, T. Pohl, T. Pattard, and J. M. Rost. "Many-body theory of excitation dynamics in an ultracold Rydberg gas". In: *Phys. Rev. A - At. Mol. Opt. Phys.* 76.1 (2007), pp. 1–10. DOI: 10.1103/PhysRevA.76.013413. arXiv: 0705.4040 (cit. on p. 38).

[37] I. Bloch. "Ultracold quantum gases in optical lattices". In: *Nat. Phys.* 1.1 (Oct. 2005), pp. 23–30. DOI: 10.1038/nphys138 (cit. on p. 43).

[38] I. Bloch, J. Dalibard, and W. Zwerger. "Many-body physics with ultracold gases". In: *Rev. Mod. Phys.* 80.3 (July 2008), pp. 885–964. DOI: 10.1103/RevModPhys.80.885 (cit. on p. 43).

[39] H. Margenau. "Van der waals forces". In: *Rev. Mod. Phys.* 11.1 (Jan. 1939), pp. 1–35. DOI: 10.1103/RevModPhys.11.1 (cit. on p. 47).

[40] J. D. Van der Waals. "Over de Continuiteit van den Gas- en Vloeistoftoestand (on the continuity of the gas and liquid state)". PhD. thesis. Leiden, 1873 (cit. on p. 47).

[41] A. Reinhard, K. C. Younge, T. C. Liebisch, B. Knuffman, P. R. Berman, and G. Raithel. "Double-Resonance Spectroscopy of Interacting Rydberg-Atom Systems". In: *Phys. Rev. Lett.* 100.23 (June 2008), p. 233201. DOI: 10.1103/PhysRevLett.100.233201 (cit. on p. 47).

[42] L. Béguin, A. Vernier, R. Chicireanu, T. Lahaye, and A. Browaeys. "Direct Measurement of the van der Waals Interaction between Two Rydberg Atoms". In: *Phys. Rev. Lett.* 110.26 (June 2013), p. 263201. DOI: 10.1103/PhysRevLett.110.263201 (cit. on p. 47).

[43] V. Sandoghdar, C. I. Sukenik, E. A. Hinds, and S. Haroche. "Direct measurement of the van der Waals interaction between an atom and its images in a micron-sized cavity". In: *Phys. Rev. Lett.* 68.23 (June 1992), pp. 3432–3435. DOI: 10.1103/PhysRevLett.68.3432 (cit. on p. 47).

[44] P. Nordlander and F. B. Dunning. "Interaction of Rydberg atoms with a metal surface in the presence of an external electric field". In: *Phys. Rev. B* 53.12 (Mar. 1996), pp. 8083–8089. DOI: 10.1103/PhysRevB.53.8083 (cit. on p. 47).

[45] A. Anderson, S. Haroche, E. A. Hinds, W. Jhe, and D. Meschede. "Measuring the van der Waals forces between a Rydberg atom and a metallic surface". In: *Phys. Rev. A* 37.9 (May 1988), pp. 3594–3597. DOI: 10.1103/PhysRevA.37.3594 (cit. on p. 47).

[46] M. Fichet, G. Dutier, A. Yarovitsky, P. Todorov, I. Hamdi, I. Maurin, S. Saltiel, D. Sarkisyan, M.-P. Gorza, D. Bloch, and M. Ducloy. "Exploring the van der Waals atom-surface attraction in the nanometric range". In: *Europhys. Lett.* 77.5 (Mar. 2007), p. 54001. DOI: 10.1209/0295-5075/77/54001 (cit. on p. 47).

[47] M. Archimi. "Real-space measurement of the mechanical effect of the van der Waals-force on Rydberg atoms". Master Thesis. Università degli Studi di Pisa, 2015 (cit. on pp. 48, 63, 72).

[48] M. Saffman, T. G. Walker, and K. Mølmer. "Quantum information with Rydberg atoms". In: *Rev. Mod. Phys.* 82.3 (Aug. 2010), pp. 2313–2363. DOI: 10.1103/RevModPhys.82.2313 (cit. on p. 50).

[49] T. G. Walker and M. Saffman. "Consequences of Zeeman degeneracy for the van der Waals blockade between Rydberg atoms". In: *Phys. Rev. A* 77.3 (Mar. 2008), p. 032723. DOI: 10.1103/PhysRevA.77.032723 (cit. on p. 50).

[50] D. Ciampini. "Realization of a 87Rb Bose-Einstein Condensate: Atomic Physics with Coherent Matter Waves". PhD Thesis. Università degli Studi di Pisa, 2002 (cit. on p. 53).

[51] M. M. Valado. "Exploring strongly correlated Rydberg excitations in cold gases using full counting statistics". PhD Thesis. Università degli Studi di Pisa, 2015, p. 169 (cit. on p. 53).

[52] H. J. Metcalf and P. van der Straten. *Laser Cooling and Trapping*. Graduate Texts in Contemporary Physics. New York, NY: Springer New York, 1999. DOI: 10.1007/978-1-4612-1470-0 (cit. on p. 53).

[53] N. Malossi, M. M. Valado, S. Scotto, P. Huillery, P. Pillet, D. Ciampini, E. Arimondo, and O. Morsch. "Full Counting Statistics and Phase Diagram of a Dissipative Rydberg Gas". In: *Phys. Rev. Lett.* 113.2 (July 2014), p. 023006. DOI: 10.1103/PhysRevLett.113.023006 (cit. on p. 54).

[54] C. Simonelli. "Studi sperimentali di eccitazioni di stati di Rydberg fortemente correlate in gas ultrafreddi". Master Thesis. Università degli Studi di Pisa, 2014 (cit. on p. 54).

[55] J. Bezanson, A. Edelman, S. Karpinski, and V. B. Shah. "Julia: A Fresh Approach to Numerical Computing". In: *CoRR* abs/1411.1 (2014), p. 41. arXiv: 1411.1607 (cit. on p. 72).

[56] T. Knopp. "Experimental Multi-threading Support for the Julia Programming Language". In: *2014 First Work. High Perform. Tech. Comput. Dyn. Lang.* IEEE, Nov. 2014, pp. 1–5. DOI: 10.1109/HPTCDL.2014.11 (cit. on p. 72).

[57] V. Garcia, E. Debreuve, and M. Barlaud. "Fast k nearest neighbor search using GPU". In: *2008 IEEE Comput. Soc. Conf. Comput. Vis. Pattern Recognit. Work.* IEEE, June 2008, pp. 1–6. DOI: 10.1109/CVPRW.2008.4563100. arXiv: 0804.1448 (cit. on p. 72).

[58] B. Lubachevsky. "Efficient parallel simulations of dynamic Ising spin systems". In: *J. Comput. Phys.* 75.1 (1988), pp. 103–122. DOI: 10.1016/0021-9991(88)90101-5 (cit. on p. 72).